Published for SISSA by Springer

Received: *October 29, 2024*
Revised: *January 13, 2025*
Accepted: *January 20, 2025*
Published: *February 18, 2025*

Measurement of the CKM angle γ in $B^{\pm} \to DK^{*}(892)^{\pm}$ decays

The LHCb collaboration

E-mail: resmi.pk@cern.ch

Abstract: Measurements of CP observables and the CKM angle γ are performed in $B^{\pm} \to DK^{*}(892)^{\pm}$ decays, where D represents a superposition of D^0 and $\overline{D}^0$ states, using the LHCb dataset collected during Run 1 (2011–2012) and Run 2 (2015–2018). A study of this channel is presented with the D meson reconstructed in two-body final states $K^{\pm}\pi^{\mp}$, K^+K^- and $\pi^+\pi^-$; four-body final states $K^{\pm}\pi^{\mp}\pi^{\pm}\pi^{\mp}$ and $\pi^+\pi^-\pi^+\pi^-$; and three-body final states $K^0_S\pi^+\pi^-$ and $K^0_S K^+K^-$. This analysis includes the first observation of the suppressed $B^{\pm} \to [\pi^{\pm}K^{\mp}]_D K^{*\pm}$ and $B^{\pm} \to [\pi^{\pm}K^{\mp}\pi^{\pm}\pi^{\mp}]_D K^{*\pm}$ decays. The combined result gives $\gamma = (63 \pm 13)^{\circ}$.

Keywords: B Physics, CKM Angle Gamma, CP Violation, Hadron-Hadron Scattering

ArXiv ePrint: 2410.21115

This paper is dedicated to the memory of our friend and colleague, Dr. Arnau Brossa Gonzalo, whose promising career was tragically cut short.

https://doi.org/10.1007/JHEP02(2025)113

Contents

1 Introduction

A precise determination of the Cabibbo-Kobayashi-Maskawa (CKM) [1, 2] angle γ is essential to test the description of *CP* violation in the Standard Model (SM). This SM parameter is determined in the interference between processes involving the transitions $b \to c\bar{u}s$ and $b \to u\bar{c}s$. The decay channels most sensitive to these interference effects are $B^{\pm} \to DK^{\pm}$ decays, where the D meson is a superposition of D^0 and $\overline{D}^0$ mesons that decay to the same final state. These tree-level decays provide a direct measurement of γ that is unaffected by the presence of physics beyond the SM (BSM), except in models where BSM enters as a charged current in tree-level decays. Direct measurements can be compared to an indirect determination of γ, which is calculated from the assumption of unitarity and measurements of other parameters in the CKM matrix.

The world average value determined by the HFLAV group is $\gamma = (66.4^{+2.8}_{-3.0})^{\circ}$ [3], which is dominated by inputs from LHCb [4]. Global fits performed by the CKMfitter and UTfit groups, where all the direct determinations are excluded, return the value $\gamma = (66.29^{+0.72}_{-1.86})^{\circ}$ [5] and $\gamma = (64.9 \pm 1.4)^{\circ}$ [6], respectively. The current uncertainty on the direct measurement remains larger than that of the indirect determination. This is due to the small branching fraction of decays sensitive to γ. This paper presents a measurement of γ using $B^{\pm} \to DK^{*\pm}$ decays, where $K^{*\pm}$ refers to the $K^{*}(892)^{\pm}$ resonance. This decay has a similar branching fraction and sensitivity to γ as $B^{\pm} \to DK^{\pm}$ channel which is the leading component in the

JHEP02(2025)113

world average [7–9]. At the LHCb experiment, the observed yields of $B^{\pm}\to DK^{*\pm}$ decays are lower than those of $B^{\pm}\to DK^{\pm}$ due to the differences in reconstruction efficiency between a $K^{*\pm}$ and $K^{\pm}$ meson. The former is reconstructed through the decay $K^{*\pm}\to K^0_S(\to\pi^+\pi^-)\pi^{\pm}$ which requires the reconstruction of an additional K^0_S meson. Nonetheless, the extremely low level of backgrounds makes this decay attractive for further study. It has been previously analysed by the B factories with two- and three-body D final states. The Belle collaboration has studied the decay $D\to K^0_S\pi^+\pi^-$ [10], whereas the BaBar collaboration has analysed a range of D decays [11, 12]. A set of two- and four-body D decays have already been investigated at LHCb [13] with a dataset corresponding to an integrated luminosity of 4.8 fb^{-1} at centre-of-mass energies $\sqrt{s}$ = 7, 8 and 13 TeV.

This paper makes use of a mixture of D-decay final states that can be grouped into three categories: *CP* eigenstates K^+K^-, $\pi^+\pi^-$ and quasi-*CP* eigenstate $\pi^+\pi^-\pi^+\pi^-$, the self-conjugate states $K^0_S\pi^+\pi^-$ and $K^0_SK^+K^-$, collectively referred to as $K^0_Sh^+h^-$, and states that are of definite strangeness, $K^-\pi^+$, π^-K^+, $K^-\pi^+\pi^-\pi^+$ and $\pi^-K^+\pi^-\pi^+$. Quasi-*CP* eigenstates refer to D-decay modes which are not pure *CP* eigenstates, but can be treated as though they were as long as the *CP*-even fraction is known and accounted for. For the D-decay modes with definite strangeness, where the charge of the kaon is the same as the B-meson charge, the decay modes are referred to as same sign (SS) and denoted as $D\to K\pi$ or $D\to K\pi\pi\pi$. When the kaon and B-meson charges are opposite, the decay modes are referred to as opposite sign (OS) and denoted as $D\to\pi K$ or $D\to\pi K\pi\pi$. The OS decay modes are suppressed with respect to SS modes. The *CP*-violation-sensitive observables are measured independently for each decay channel. Then they are combined to obtain the value of the angle γ. This measurement uses the LHCb dataset of proton-proton (pp) collisions collected during Run 1 (2011–2012) and Run 2 (2015–2018), corresponding to an integrated luminosity of 9 fb^{-1} at centre-of-mass energies $\sqrt{s}$ = 7, 8 and 13 TeV.

The measurement strategies for the different decay channels are given in section 2. The LHCb detector is described in section 3 and the selection of $B^{\pm}\to DK^{*\pm}$ candidates is detailed in section 4. Section 5 elaborates the backgrounds that are present after selection followed by the details of signal yields for each mode in section 6. The determination of *CP*-violating observables is described in section 7. Systematic uncertainties are discussed in section 8. The results and their interpretation are shown in section 9.

2 Analysis overview

The amplitude of a B^- decay to D^0K^{*-} decay is defined as

$$\mathcal{A}(B^-\to D^0K^{*-})\equiv A_B, \tag{2.1}$$

and that of a B^- decay to $\overline{D}^0K^{*-}$ decay is given as

$$\mathcal{A}(B^-\to \overline{D}^0K^{*-}) = A_B\cdot r_B\cdot e^{i(\delta_B-\gamma)}, \tag{2.2}$$

where r_B is the ratio of the magnitudes of the amplitudes of $B^-\to\overline{D}^0K^{*-}$ and $B^-\to D^0K^{*-}$ and δ_B is the corresponding strong-phase difference between them. When the D meson decays to a state that is accessible from both the D^0 and $\overline{D}^0$ meson, there is interference between the two decay paths. This interference gives access to the CKM angle γ. Analogous expressions can be formed for the charge-conjugate B^+ decay where the sign of the γ angle is flipped ($\gamma \leftrightarrow -\gamma$). The measurement strategies for the various types of D decays are described in detail in this section.

The amplitudes for the D^0 and the $\overline{D}^0$ mesons decaying to CP eigenstates are the same.[1] Hence, the difference in the two overall amplitudes is driven by the difference in the two B-meson amplitudes. This leads to a relatively small amount of CP violation that is of the order of r_B. A coherence factor κ is defined, satisfying $0 \leq \kappa \leq 1$, which quantifies the dilution of the interference effects of interest due to selected $B^\pm \to DK^0_S\pi^\pm$ decays that do not proceed through the intermediate $K^*(892)^\pm$ resonance. The value of κ is estimated in ref. [13] to be 0.95 ± 0.06. A coherence value of one would represent a pure resonant sample.

Measurements with CP eigenstates are performed according to the formalism presented in refs. [14, 15]. This includes obtaining the asymmetries between the rates of B^+ and B^- decays and ratios with SS decays that are directly related to the physics parameters of interest. The technique can be extended to quasi-CP eigenstates provided the CP-even fraction of the final state, F_{CP}, is known [16] and accounted for, as given in eqs. (2.3) and (2.4). For $B^\pm \to DK^{*\pm}$, when the D meson decays to a final state X, the ratio R^X_{CP} is defined as

$$\begin{aligned} R^X_{CP} &= \frac{\Gamma(B^- \to [X]_D K^{*-}) + \Gamma(B^+ \to [X]_D K^{*+})}{\Gamma(B^- \to [SS]_D K^{*-}) + \Gamma(B^+ \to [SS]_D K^{*+})} \times \frac{\mathcal{B}(D^0 \to SS)}{\mathcal{B}(D^0 \to X)} \\ &= 1 + r_B^2 + 2\kappa(2F^X_{CP} - 1) r_B \cos\delta_B \cos\gamma, \end{aligned} \tag{2.3}$$

and the asymmetry A^X_{CP} as

$$\begin{aligned} A^X_{CP} &= \frac{\Gamma(B^- \to [X]_D K^{*-}) - \Gamma(B^+ \to [X]_D K^{*+})}{\Gamma(B^- \to [X]_D K^{*-}) + \Gamma(B^+ \to [X]_D K^{*+})} \\ &= \frac{2\kappa(2F^X_{CP} - 1) r_B \sin\delta_B \sin\gamma}{R^X_{CP}}. \end{aligned} \tag{2.4}$$

For $D \to KK$ and $D \to \pi\pi$, the CP-even fraction is one. For $D \to \pi\pi\pi\pi$, the CP-even fraction has been measured at the BESIII experiment to be 0.735 ± 0.016 [17]. The ratio R^X_{CP} and asymmetry A^X_{CP} are measured for each D-meson decay mode that is a (quasi)-CP eigenstate, and the SS decay chosen for the normalisation in the denominator of eqs. (2.3) and (2.4) is the one with the same multiplicity as the (quasi-)CP eigenstate.

The formalism for measuring γ using the OS and SS D-meson decays is given in refs. [18, 19]. For the OS decay channels, the two amplitudes from the B decay to the final state are of similar size, resulting in maximum interference. In this formalism, the hadronic properties of the D decay become relevant to the interpretation of the ratios with SS decays and asymmetries between B^+ and B^- decays. The hadronic parameters are defined as r^X_D, δ^X_D, and κ^X, where X is the final state, r^X_D is the ratio of the suppressed and favoured D-decay amplitudes, δ^X_D is the average strong-phase difference between them and κ^X_D takes into account the variation of δ^X_D over the phase space which dilutes the interference. Since

[1]Violation of CP symmetry in D decays is neglected. This effect is much smaller compared to CP violation in the B-meson decay.

$D \to K\pi$ is a two-body decay, the value of κ^X is unity. The ratios and asymmetries between the OS and SS decay modes are given by

$$R^X_{OS} = \frac{\Gamma(B^- \to [OS]_D K^{*-}) + \Gamma(B^+ \to [OS]_D K^{*+})}{\Gamma(B^- \to [SS]_D K^{*-}) + \Gamma(B^+ \to [SS]_D K^{*+})} \tag{2.5}$$

$$= r_B^2 + (r_D^X)^2 + 2\kappa r_B \kappa_D^X r_D^X \cos(\delta_B + \delta_D^X)\cos\gamma, \tag{2.6}$$

$$A^X_{OS} = \frac{\Gamma(B^- \to [OS]_D K^{*-}) - \Gamma(B^+ \to [OS]_D K^{*+})}{\Gamma(B^- \to [OS]_D K^{*-}) + \Gamma(B^+ \to [OS]_D K^{*+})}$$

$$= \frac{2\kappa r_B \kappa_D^X r_D^X \sin(\delta_B + \delta_D^X)\sin\gamma}{R^X_{OS}}, \tag{2.7}$$

$$A^X_{SS} = \frac{\Gamma(B^- \to [SS]_D K^{*-}) - \Gamma(B^+ \to [SS]_D K^{*+})}{\Gamma(B^- \to [SS]_D K^{*-}) + \Gamma(B^+ \to [SS]_D K^{*+})}$$

$$= \frac{2\kappa r_B \kappa_D^X r_D^X \sin(\delta_B - \delta_D^X)\sin\gamma}{1 + r_B^2 (r_D^X)^2 + 2\kappa r_B \kappa_D^X r_D^X \cos(\delta_B - \delta_D^X)\cos\gamma}. \tag{2.8}$$

Taking expected values for r_B and r_D [5], it is clear that A^X_{SS} is small in comparison to A^X_{OS}. Hence, the sensitivity to *CP* violation in the SS decay modes is expected to be very small.

For the three-body decay modes, the variation of the strong phase δ_D over the phase space of the decay is large. This leads to values of F_{CP} close to 0.5 which maximally dilutes the interference term, and hence, measuring $R_{CP}^{K^0_S h^+ h^-}$ and $A_{CP}^{K^0_S h^+ h^-}$ will result in very little sensitivity to γ. Instead, these decays are analysed in regions of phase space to exploit regions where the coherence is high. The formalism is developed in refs. [20–22]. The final state is dependent on the kinematics of the decay products which can be visualised using the Dalitz plot method. The strong phase varies over the phase space, and the strong-phase difference at a point in phase space between the D^0 and $\overline{D}^0$ decay is given by $\Delta\delta_D$. The density of the B^- decay, P_B, at a specific point in the D phase space is expressed as

$$\begin{aligned} P_B &= |A|^2 + r_B^2|\overline{A}|^2 + r_B(A^*\overline{A}e^{i(\delta_B-\gamma)} + A\overline{A}^* e^{-i(\delta_B-\gamma)}) \\ &= |A|^2 + r_B^2|\overline{A}|^2 + 2\kappa r_B|\overline{A}||A|(\cos\Delta\delta_D\cos(\delta_B-\gamma) - \sin\Delta\delta_D\sin(\delta_B-\gamma)) \\ &= |A|^2 + r_B^2|\overline{A}|^2 + 2\kappa\sqrt{|A|^2||\overline{A}|^2}(C\,x_- - S\,y_-), \end{aligned} \tag{2.9}$$

where A and $\overline{A}$ are the amplitudes of the D^0 and $\overline{D}^0$ decays to the $K^0_S h^+ h^-$ final state, $x_- = r_B\cos(\delta_B-\gamma)$, $y_- = r_B\sin(\delta_B-\gamma)$, $C = \cos\Delta\delta_D$ and $S = \sin\Delta\delta_D$. For the charge-conjugate mode, $B^+ \to DK^{*+}$, the density is given by the same expression with $A \leftrightarrow \overline{A}$, $\gamma \leftrightarrow -\gamma$, $x_- \leftrightarrow x_+$ and $y_- \leftrightarrow y_+$, where $x_+ = r_B\cos(\delta_B+\gamma)$ and $y_+ = r_B\sin(\delta_B+\gamma)$.

The D-meson decay Dalitz plot is split into bin pairs, symmetric with respect to the $m^2_{K^0_S h^+} = m^2_{K^0_S h^-}$ axis. Bins with $m^2_{K^0_S h^-} > m^2_{K^0_S h^+}$ are given positive indices 1 to N. Those with $m^2_{K^0_S h^-} < m^2_{K^0_S h^+}$ are given negative indices such that bins i and $-i$ are *CP* conjugates. The partial decay rate in the i^{th} bin of the D-decay phase space for B^- and B^+ modes, $\Gamma_i^{\mp}$, can be found by integrating eq. (2.9) and written as

$$\Gamma_i^{\mp} = \mathcal{N}^{\pm}\left(F_{\pm i} + (r_B)^2 F_{\mp i} + 2\kappa\sqrt{F_i F_{-i}}(c_i x_{\mp} \pm s_i y_{\mp})\right). \tag{2.10}$$

Here, $F_{\pm i}$ is the fraction of observed D^0-meson decays in each bin given the experimental reconstruction and selection efficiency, and migration effects and $\mathcal{N}^{\pm}$ is the normalisation

JHEP02(2025)113

parameter. Neglecting *CP* violation in these charm decays, the charge conjugate decays satisfy $F_i = \overline{F}_{-i}$, where $\overline{F}_i$ is the fraction of observed $\overline{D}^0$ decays in the bin with index i. The c_i and s_i parameters are the amplitude-weighted averages of the functions C and S over the bin.

The values of c_i and s_i have been measured by the CLEO [23] and BESIII [24, 25] collaborations. Both have followed the same partition of the phase space. There are multiple options presented in ref. [23]. The ones used in this analysis are named the "optimal" and "2-bins" binning schemes for $D \to K^0_S\pi^+\pi^-$ and $D \to K^0_S K^+K^-$ decays, respectively. These represent the schemes that are expected to give the best sensitivity for γ under the experimental conditions for this analysis. There are in total $2 \times 8 = 16$ and $2 \times 2 = 4$ bins in the $D \to K^0_S\pi^+\pi^-$ and $D \to K^0_S K^+K^-$ modes, respectively. These schemes are followed in this analysis so that the values c_i and s_i can be directly used as external inputs. The $F_{\pm i}$ values are taken from the $B^\pm \to D(\to K^0_S h^\pm h^\mp)h^\pm$ analysis [7]. This assumes that the relative efficiency between two points on the Dalitz plot of the D decay is the same for $B^\pm \to Dh^\pm$ and $B^\pm \to DK^{*\pm}$ modes, which is verified in simulation. The use of external inputs for the strong-phase difference, rather than reliance on a model of the D-meson decay, ensures that the measurement is amplitude-model independent and does not incur systematic uncertainties due to the model, which are hard to quantify.

The SS decay modes are used as a control channel in this analysis. Their high signal yield benefits the reconstructed-mass parametrisation, which is used to model the small background contributions from $B^\pm \to D^*K^{*\pm}$ decays in the other D-decay modes. The *CP* observables are measured in the *CP* fit, consisting of a simultaneous maximum-likelihood fit performed in the different categories of the two- and four-body decays defined by the B charge and D-decay mode. The ratios and asymmetries in eqs. (2.3)–(2.8) are measured. Another fit is performed simultaneously for the three-body decays in the categories of B charge, D-decay mode and Dalitz plot bin. The *CP* observables $x_\pm$ and $y_\pm$ are extracted from this fit. The results from all sets of modes are combined to obtain a precise single solution for γ.

3 Detector and simulation

The LHCb detector [26, 27] is a single-arm forward spectrometer covering the pseudorapidity range $2 < \eta < 5$, designed for the study of particles containing b or c quarks. The detector includes a high-precision tracking system consisting of a silicon-strip vertex detector surrounding the pp interaction region [28], a large-area silicon-strip detector located upstream of a dipole magnet with a bending power of about 4 T m, and three stations of silicon-strip detectors and straw drift tubes [29, 30] placed downstream of the magnet. The tracking system provides a measurement of the momentum, p, of charged particles with a relative uncertainty that varies from 0.5% at low momentum to 1.0% at 200 GeV/c. The minimum distance of a track to a primary pp collision vertex (PV), the impact parameter (IP), is measured with a resolution of $(15 + 29/p_{\mathrm{T}})$ μm, where p_{T} is the component of the momentum transverse to the beam, in GeV/c. Different types of charged hadrons are distinguished using information from two ring-imaging Cherenkov detectors [31]. Photons, electrons and hadrons are identified by a calorimeter system consisting of scintillating-pad and preshower detectors, an electromagnetic and a hadronic calorimeter. Muons are identified by a system composed of alternating layers of iron and multiwire proportional chambers [32].

JHEP02(2025)113

The online event selection is performed by a trigger [33], which consists of a hardware stage, based on information from the calorimeter and muon systems, followed by a software stage, which applies a full event reconstruction. The events for the analysis that satisfy the hardware trigger are selected through two routes. Either they have an energy deposit in the calorimeter associated to the signal decay, or a particle not associated to the signal candidate fulfills any requirement. At the software stage, at least one particle is required to have high p_T and high χ^2_{IP}, where χ^2_{IP} is defined as the difference in the primary vertex fit χ^2 with and without the inclusion of that particle. A multivariate algorithm [34] is used to select secondary vertices consistent with being a two-, three-, or four-track b-hadron decay.

Simulation is required to model the effects of the detector acceptance and the imposed selection requirements. In the simulation, pp collisions are generated using Pythia [35] with a specific LHCb configuration [36]. Decays of unstable particles are described by EvtGen [37], in which final-state radiation is generated using Photos [38]. The interaction of the generated particles with the detector, and its response, are implemented using the Geant4 toolkit [39] as described in ref. [40].

4 Candidate selection

All tracks and decay vertices are required to be of good quality, and the reconstructed mass of the K^0_S, D and $K^{*\pm}$ candidates must be close to their known values [41]. The K^0_S candidates are formed from two oppositely charged pion tracks that are reconstructed either using hits in the vertex detector and downstream tracking stations, or only the latter. These track types are referred to as *long* and *downstream*, respectively. Requirements are placed on the reconstructed K^0_S mass to be within $\pm 15(20)\,\text{MeV}/c^2$ of the known mass for *long* (*downstream*) candidates. The D-meson candidates are reconstructed in two-, four- and three-body final-state categories, labelled $D \to hh$, $D \to 4h$, and $D \to K^0_\text{S}hh$.

In the case of $D \to hh$ decays, the D-meson candidate is formed by combining two oppositely charged tracks. Particle identification (PID) requirements are placed on the kaons and pions in such a way that each pair of tracks can only appear in one D-meson decay sample. The particle selection does not sufficiently suppress the double misidentification of $K^-\pi^+$ as π^-K^+, which peaks at the D-meson mass. Candidates in the OS sample are removed if the measured D-meson mass, when reconstructed under the double misidentification hypothesis, falls within $\pm 15\,\text{MeV}/c^2$ of the known D-meson mass [41]. The corresponding selection is not made in the SS sample since here the contamination rate is very low.

For the $D \to 4h$ decays, two positively and two negatively charged tracks are combined. PID requirements are placed on the kaons. In the case of $D \to K\pi\pi\pi$, PID requirements are only imposed on those pion candidates that have the opposite charge of the kaon. Additional PID selection on the other pion would result in lower signal efficiency without any significant reduction in misidentified backgrounds. A mass veto of $\pm 15\,\text{MeV}/c^2$ around the known D-meson mass is placed on the OS samples to reduce doubly misidentified background. In the case of the $D \to \pi\pi\pi\pi$ decay, only the two pions with opposite charge to the parent B meson have PID requirements applied. This is sufficient to reduce misidentified decays to a negligible level. Furthermore, candidates are vetoed if the reconstructed mass of any oppositely charged pair of pions is within the range 480–505 MeV/c^2 to remove background from $D \to K^0_\text{S}\pi\pi$.

For $D \to K^0_S hh$ decays the candidate is formed by combining a K^0_S candidate with two oppositely charged tracks, where additionally the K^0_S mass is constrained to its known value in a kinematic fit [42]. For the two tracks originating from the D-meson vertex, PID requirements are placed to reduce background from $D \to K^0_S K^+\pi^-$ decays, semileptonic D decays, and decays in flight of hadrons to leptons. In all cases the reconstructed mass of the D-meson candidate is required to be within $\pm 25\,\text{MeV}/c^2$ of the known mass [41].

A candidate $K^{*\pm}$ meson is reconstructed by combining a K^0_S and a companion pion. The reconstructed mass is required to be within $\pm 75\,\text{MeV}/c^2$ of the known $K^{*\pm}$ mass [41]. The D-meson candidate is combined with the $K^{*\pm}$ to form the $B^\pm$-meson candidate. To suppress background from $B^\pm \to DK^0_S K^\pm$ decays, PID requirements are placed on the companion pion. Background from nonresonant $B^\pm \to DK^0_S\pi^\pm$ decays is reduced by using the properties of the vector-particle decay. The helicity angle θ is defined as the angle between the vectors of the companion K^0_S meson and the B momentum in the $K^{*\pm}$ rest frame. It is required that $|\cos\theta| > 0.3$.

A requirement is placed on the displacement of the D-meson vertex from the B-meson vertex to reduce background from B decays to the final-state particles without the intermediate D meson. A displacement requirement from their parent meson is also applied to any *long* K^0_S meson vertex. This removes background from $B^\pm \to D\pi^\pm\pi^\mp\pi^\pm$ decays and suppresses the reconstruction of $D \to \pi^\pm\pi^\mp h^\pm h^\mp$ as $D \to K^0_S h^\pm h^\mp$. Finally, the reconstructed B-meson mass is computed applying mass constraints to the D and the K^0_S mesons in each decay chain, and constraining the B meson to originate from the primary vertex.

A separate boosted decision tree (BDT) classifier [43, 44] is trained for each multiplicity of D-meson decay to separate signal from background. The BDTs are trained using simulation to provide the signal distributions and candidates in the upper sideband of reconstructed B mass in data are used to provide the background distributions. The upper sideband is defined with reconstructed B mass in the range $5800 - 6100$ MeV/c^2 for three-body D decays and $5400 - 5800$ MeV/c^2 for two- and four-body D decays. For $D \to K^0_S hh$ decays the variables used in the training are those in ref. [7] with the addition of kinematic variables p and p_T for the companion K^0_S meson. Studies on simulations have shown that a similar relative efficiency over the D-meson phase space, which allows the use of the F_i parameters measured in ref. [7]. Similar variables are used for the two- and four-body D-meson decays. A k-fold of two is used to avoid any sculpting of the final upper sideband distribution [45] since the training sample and fit sample are not mutually exclusive.

Selection requirements on the BDT classifiers are placed based on the optimisation of the sensitivity to the *CP* observables. Pseudoexperiments are generated with total yields corresponding to different selection values for the output of the BDT classifier and *CP* observables are determined in each of them as described in section 7. The criterion that gives the best precision on *CP* observables is chosen. The resulting BDT selection requirement is different for the OS and (quasi-)*CP* eigenstates, the SS decay modes and the $D \to K^0_S hh$ decays. The signal selection efficiency is higher than 90% for each BDT classifier.

5 Background determination

For each decay channel, data from the *long* and *downstream* K^0_S categories are combined. Due to the impact of the mass constraints, the effect of the different resolutions of the reconstructed K^0_S mass in these decays is reduced, and the differences in the reconstructed-mass distributions of signal decays are negligible. A notable background for $B^\pm \to DK^\pm$ decays is $B^\pm \to D\pi^\pm$ with a pion misidentified as a kaon. The corresponding background in $B^\pm \to DK^{*\pm}$ decays is $B^\pm \to D\rho^\pm$, but since the subsequent decay is different, it does not enter the sample.

The two- and four-body SS decay channels have the highest signal yields. From the distributions shown in figures 1 and 2, it is seen that the signal peak is well separated from $B \to D^* K^*$ decays that are found at lower reconstructed mass due to the missing pion or photon which is not reconstructed. These are called partially reconstructed backgrounds (PRB). Therefore, the *CP* observables are determined using a fit to the B-meson reconstructed mass distribution, $m_{\rm rec}$, in the range 5230–5600 MeV/c^2. This removes most of the PRB contribution. The combinatorial background level is also low. In order to determine the yield of the PRB candidates that pass the selection, a fit of the SS decay channel is performed over a wider fit range. The PRB decays have negligible *CP* violation in this channel, and therefore their distributions can be fit reliably using simulation and two fit parameters to determine the relative fractions of the different components that make up these decays. This is not the case in decay modes with higher rates of *CP* violation as there are three amplitudes in the $B^\pm \to D^{*0} K^{*\pm}$ decays, each with its own strong phase difference. Two of these amplitudes have identical distributions of $m_{\rm rec}$ and hence it is not possible to separate them using this fit, nor to measure the *CP*-violating parameters of the $B^\pm \to D^{*0} K^{*\pm}$ decays. Instead, the total yield of PRB contribution in the SS candidates is fit, and the fraction leaking above a $m_{\rm rec}$ value of 5230 MeV/c^2 is determined. The PRB yield in other decay channels is estimated by taking this yield and scaling by the branching fractions and selection efficiency ratios. The effect of this assumption is assessed as a systematic uncertainty.

The fit of the $m_{\rm rec}$ distribution of SS decay modes is performed as an unbinned extended maximum-likelihood fit. The probability density function (PDF) for the signal shape is given by the sum of a Gaussian and a modified Cruijff function [7] defined as

$$f(m_{\rm rec}) \propto \begin{cases} \exp\left[\frac{-(m_{\rm rec}-\mu)^2\left(1+\beta(m_{\rm rec}-\mu)^2\right)}{2\sigma^2+\alpha_L(m_{\rm rec}-\mu)^2}\right] & \text{if } m_{\rm rec}-\mu<0, \\ \exp\left[\frac{-(m_{\rm rec}-\mu)^2\left(1+\beta(m_{\rm rec}-\mu)^2\right)}{2\sigma^2+\alpha_R(m_{\rm rec}-\mu)^2}\right] & \text{if } m_{\rm rec}-\mu>0. \end{cases} \tag{5.1}$$

The parameters μ and σ are shared between these two components. The tail parameters α_L, α_R and β of the modified Cruijff function are determined from simulation. In the fit to data the mean, width, and signal yield are freely varied. Combinatorial background is modelled by an exponential function and the slope and yield are determined in the fit to data. The PRB candidates to the left of the signal peak are modelled as in ref. [46]. The results of the fit for the two- and four-body SS decays are shown in figures 1 and 2, respectively. The yield of the PRB candidates in the region above 5230 MeV/c^2 is 25 ± 1 in the two-body SS decay mode and 17 ± 1 in the four-body SS decay mode. The yield of the PRB candidates in the

JHEP02(2025)113

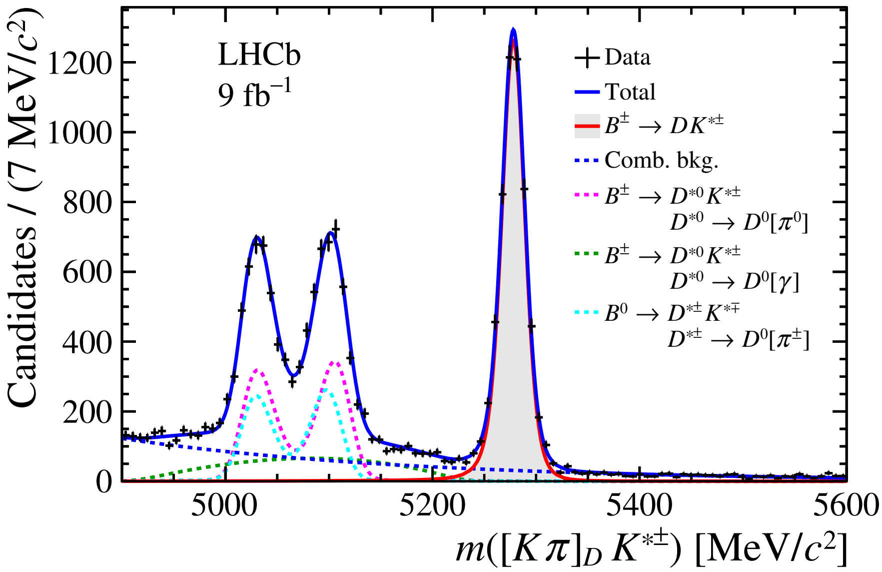

Figure 1. Reconstructed-mass ($m_{\rm rec}$) distribution of the two-body favoured (SS) mode $K\pi$ with the fit result superimposed, using the full Run 1 and Run 2 datasets. In the legend, missing particles which are not reconstructed are shown inside square brackets.

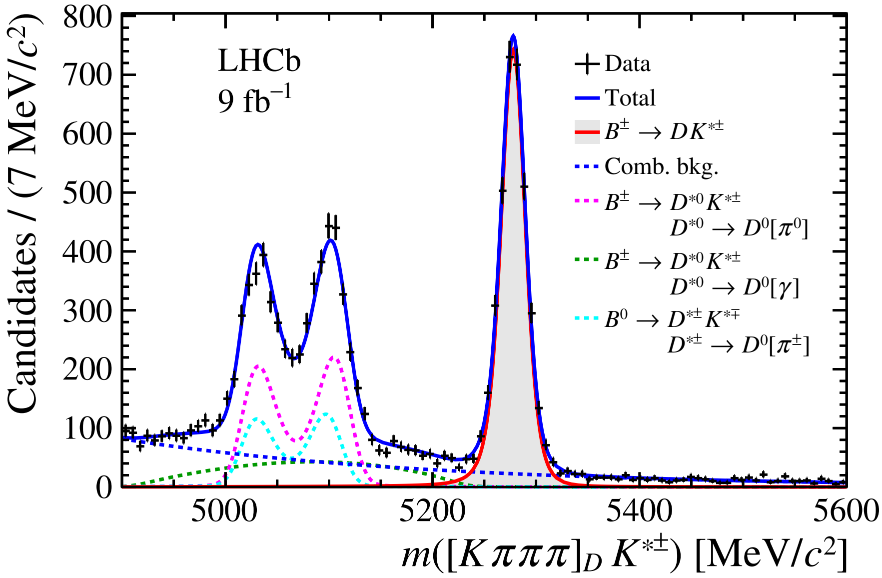

Figure 2. Reconstructed-mass ($m_{\rm rec}$) distribution of the four-body favoured (SS) mode $K\pi\pi\pi$ with the fit result superimposed, using the full Run 1 and Run 2 dataset. In the legend, missing particles which are not reconstructed are shown inside square brackets.

other decay channels is determined by scaling the yield in the SS decay by the appropriate D decay branching-fraction ratio and selection efficiencies.

In certain channels, there are further peaking backgrounds under or near the signal peak that need to be accounted for in the fit. One is the decay of a B meson to the same final state as the signal, but with no intermediate charm meson. This charmless background is reduced by the requirement that the D-meson vertex is displaced from that of the B

meson. This background is studied by examining events in the region 1910–1960 MeV/c^2 of D-meson reconstructed mass. Significant yields of this background remain in the $D \to \pi\pi$ and $D \to \pi\pi\pi\pi$ channels. They are determined by fits to the distributions of reconstructed B mass in the D-meson higher mass sidebands, separately for each B charge. The mean and width in these fits are obtained from data. The shape of the background is similar to, but wider than, the signal.

Background from $\Lambda_b^0 \to \Lambda_c^+(\to pK^-[\pi^+])K^{*-}$ decays can contribute under the signal peak in m_{rec} distribution for the $D \to K^+K^-$ decay mode when the pion from the Λ_c^+ is missed in the reconstruction and the proton is misidentified as a kaon. The shape of this background is determined from a fit to the reconstructed-mass distribution of simulated $\Lambda_b^0 \to \Lambda_c^+ K^{*-}$ decays, that are reconstructed in the same way as the signal decays, with an extended Cruijff function used to model it. The yield of this background is determined relative to the signal yield taking into account the relative production ratios of the Λ_b^0 and $B^\pm$ hadrons [47], the ratio of branching fractions of the signal and background decays [41] and the relative efficiency of selecting the background in comparison to the signal decay mode. As no large *CP* violation is observed in baryons, this background is assumed to occur equally for B^+ and B^- decays and is approximately 2% of the signal yield for the $D \to K^+K^-$ mode.

Decays of the type $B_s^0 \to \overline{D}^0\overline{K}^{**0}$, with $\overline{K}^{**0} \to K^{*-}[\pi^+]$ and $K^{*-} \to K_S^0\pi^-$, where the pion from the $\overline{K}^{**0}$ decay is missed and not reconstructed, can appear in the region below the signal peak in m_{rec} distribution. These decays are favoured in the OS modes considered in this measurement, where low signal yields are expected. These backgrounds are suppressed in the SS decay modes and hence the yield of this B_s^0 background cannot be determined from the SS sample. Instead the B_s^0 background is determined from the lower sideband of the OS samples using candidates with m_{rec} in the range 4900–5230 MeV/c^2 with both $B^\pm$ charges combined. The process is carried out separately for the two and four body channels. The candidates in this sideband are assumed to be either combinatorial background, PRB, or the B_s^0 background of interest. Using the technique of background subtraction, the combinatorial background and PRB are removed from the sample. The m_{rec} distribution and yield of the combinatorial background to be subtracted is determined from a fit to candidates with m_{rec} above 5400 MeV/c^2. The m_{rec} distribution for the PRB candidates is taken from the fit in figure 1. The PRB yield in the OS sample is determined by the multiplying the corresponding yield in the SS sample by the ratio R_{OS}^X in eq. (2.6), which is determined using physics input values from ref. [4]. While values of r_B and δ_B are not correct for the $B \to D^*K^*$ decays, the final impact of these choices results in a small systematic uncertainty. After subtraction, the remaining distribution in the OS sideband is assumed to be solely from B_s^0 decays. Fast simulation [48] is used to generate samples of $B_s^0 \to \overline{D}^0\overline{K}^{**0}$ decays, where $\overline{K}^{**0}$ is one of the following resonances: $\overline{K}_1(1270)^0$, $\overline{K}_1(1400)^0$, $\overline{K}^*(1410)^0$, $\overline{K}^*(1430)^0$ and $\overline{K}_2^*(1430)^0$. The resulting m_{rec} shape is similar and averaged over the five resonances. This shape is used to fit the OS sideband and determine the expected yield of the B_s^0 background above 5230 MeV/c^2. For the two-body OS channel this is 2.5 candidates summed over both charges. Any *CP* violation in these B_s^0 decays is assumed to be negligible [46], and hence 1.25 candidates of this background are assigned to each charge. The corresponding yield of the B_s^0 background in the four-body OS decay channel is 2. The size of the B_s^0 background in the other decay channels can be found by scaling 2.5 by the appropriate ratio of D-decay branching fractions and selection efficiencies. In these other channels the B_s^0 background yield is negligible and therefore are not considered further.

6 Signal yields and observation of decays

Signal yields are estimated from an unbinned simultaneous maximum-likelihood fit to m_{rec}, where the categories are the D-meson decay channel and B-meson charge. The mass range is reduced to 5230–5600 MeV/c^2 to remove the partially reconstructed $B \to D^* K^*$ backgrounds. The two main components of the fit are the signal and the combinatorial background. The signal is modelled by the same function used in the fit with a wider mass range in figures 1 and 2, where the mean and width are freely varying. The two-body decay categories of the D meson all share the same mean and width. The same is the case for the four-body D-decay categories. For the three-body decay categories, the signal function is simplified and consists only of the modified Cruijff PDF shown in eq. (5.1). The μ and σ parameters are freely varying and shared across the three-body decay categories with the tail parameters determined from simulation. The tail parameters are shared across both the $K_S^0 hh$ mdoes. The combinatorial background is modelled by an exponential PDF. The yield of this background is freely varying in each category. The slope of the exponential PDF is shared between the two- and four-body categories, which is valid as seen from the fits in figures 1 and 2. For the small residual PRB contribution, the yield and shape are described in section 5. Backgrounds specific to certain decay channels described in section 5 are also included.

The results of this fit are given in table 1. As expected, there are large signal yields in the SS two- and four-body decay modes, approximately 2.5 times larger than those in ref. [13]. This is due to the inclusion of data collected in 2017 and 2018. The signal yield of the B decay where $D \to K_S^0 \pi\pi$ is an order of magnitude larger than that analysed at Belle [10] and around three times that analysed at BaBar [11]. A further fit is performed where the OS decay modes have both charges combined. Using Wilks' theorem [49], it is found that the statistical significance of an observation for πK and $\pi K \pi\pi$ is above five standard deviations. This is the first observation of the suppressed $B^\pm \to [\pi^\pm K^\mp]_D K^{*\pm}$ and $B^\pm \to [\pi^\pm K^\mp \pi^\pm \pi^\mp]_D K^{*\pm}$ decays.

7 Determination of *CP*-violating observables

The *CP*-violating observables are determined through simultaneous fits to the reconstructed-mass distributions where the events are separated by category. For the two- and four-body decays, the categories are each D-decay mode, separated into B^+ and B^- candidates. The three-body decay modes are further separated into the defined bins on the Dalitz plot.

The signal yields in this simultaneous fit to the different mass distributions are expressed in terms of the *CP*-violating parameters, which allows the direct determination of their statistical correlations and eases the subsequent determination of common systematic uncertainties. Corrections are included in the fit to take into account $B^\pm$ production asymmetries and detection asymmetries for $K^\pm$ and $\pi^\pm$. The $B^\pm$ production asymmetry, $A_{B^+} = (+0.028 \pm 0.068)\%$, is taken from ref. [50]. The kaon detection asymmetry A_{K^+} is mainly due to the nuclear

JHEP02(2025)113

D decay mode	B^-	B^+	Purity (%)
$K\pi$	2656 ± 55	2844 ± 57	94
KK	366 ± 20	274 ± 18	90
$\pi\pi$	121 ± 13	63 ± 10	69
πK	5 ± 4	35 ± 7	58
$K\pi\pi\pi$	1665 ± 44	1783 ± 45	93
$\pi\pi\pi\pi$	160 ± 14	149 ± 14	77
$\pi K\pi\pi$	13 ± 5	18 ± 5	58
$K^0_S\pi\pi$	279 ± 18	268 ± 18	85
$K^0_S KK$	29 ± 6	40 ± 7	86

Table 1. Summary of the observed signal yields for each D-decay channel and for each B-meson charge. The uncertainties are statistical only. The purity in the mass region 5230–5330 MeV/c^2 is also given for both the charges combined.

interaction length difference between K^+ and K^- coming from differences in the interaction with the material as they pass through the LHCb detector. This is corrected using the difference in detection asymmetries between kaons and pions, $A_{K^+\pi^-} = (-0.960 \pm 0.134)\%$, which is defined such that a higher $K^+\pi^-$ detection efficiency leads to a positive asymmetry. The pion detection asymmetry A_{π^-} is corrected using $A_{\pi^-} = (-0.064 \pm 0.019)\%$, where the uncertainty includes systematic effects [51].

The raw asymmetry A_{raw} from the signal yields of B^+ and B^- decays is made of the CP asymmetry A^X_{CP} and the asymmetry corrections A_{corr} as

$$A_{\text{raw}} = A^X_{CP} + A_{\text{corr}}. \tag{7.1}$$

In the case of the two- and four-body decay modes the signal yield in each decay mode and each charge is reparametrised in terms of the CP-violating observables, the production and detection asymmetries, the signal yield of the SS decay that has the same D-decay final-state multiplicity and efficiency ratios. These efficiency ratios take into account the differences in selection between the signal channel and the relevant SS decay channel. The efficiency is determined through simulation except for the efficiency of PID requirements which is determined using a data-driven method [52].

In the case of the three-body decay modes, there are two separate free normalisation parameters for the two B-meson charges. This means that the result is independent of production and detection asymmetries. The signal yields in each bin are parametrised using eq. (2.10), where the two normalisation parameters $\mathcal{N}^{\pm}$ are set up to be the total B^+ and B^- yield integrated over the phase space for each decay channel. The F_i parameters are those determined in ref. [7]. The values of c_i and s_i are determined by BESIII in refs. [24, 25] which include a combination with the results from CLEO [23] and are fixed in the fit. The PDF describing the m_{rec} in each category is the same as for the data combined across phase space. The tail parameters are the same in each Dalitz plot bin and fixed from simulation.

JHEP02(2025)113

The differences between each bin are negligible. The mean mass and width are shared across the categories. The slope of the combinatorial background is fixed from the fit integrated over phase space and is the same in each Dalitz plot bin. This simplification is motivated through inspection of the data and has negligible associated systematic uncertainty. However, the combinatorial yield is determined by the fit separately for each Dalitz plot bin. The yield of PRB candidates integrated over phase space is determined from scaling the yield observed in the $D \to K\pi$ SS decay. In a B^- decay it is assumed that the PRB candidates contains a D^0, and hence the yield of this background is distributed according to the F_i values over the phase space with this assumption. As the estimated yield of the PRB candidates in the $K^0_S\pi\pi(K^0_S KK)$ decay category after selection is 6(1), the impact of this assumption is negligible. Hence, the free parameters that describe the data are the mean and width of the signal, the total yield of B^+ and B^- for each decay channel, the yield of combinatorial background in each category, and the *CP*-violating observables $x_\pm$ and $y_\pm$.

The fits for all decay modes are tested through pseudoexperiments to assess any fit bias. No bias is found and the uncertainties are found to be well estimated for the two- and four-body decay modes. In the case of the three-body decay modes there is evidence of a small bias of up to 7% of the statistical uncertainty. The source of the bias is determined to be due to the very low signal yields that occur in some categories. The fit results are corrected for this small bias.

The results of the fit for the two- and four-body decay modes are shown in figures 3–5, with numerical results provided in section 9. There are small asymmetries within the SS sample, as expected by the physics parameters, with noticeably larger values for the OS and (quasi)-*CP*-eigenstate decay channels, although not all are statistically significant. The results of the three-body decay modes are visually presented in figure 6, where the $x_\pm$ and $y_\pm$ are shown. The opening angle between the two vectors joining the central values to the origin is 2γ. To investigate the goodness-of-fit in the three-body decay channels, a further fit is run, where the signal yield is not parametrised in terms of the fit observables described above, but freely varying in each category. Asymmetries are calculated and shown in figure 7. The asymmetries are calculated in effective bin pairs, labelled i, that compare the yield of B^- decays in a bin i with the yield of B^+ decays in a bin $-i$. Also shown are the expected asymmetries given the fitted values of $x_\pm$ and $y_\pm$. The agreement is good between the two approaches with a χ^2 value of 1.6 per degree of freedom and this demonstrates that the system of equations used to fit the data is reasonable.

8 Systematic uncertainties

Several sources of systematic uncertainties affect the measurement. Two methods are used to compute the systematic uncertainties on the *CP* observables. To evaluate the uncertainty due to parameters that are kept constant in the fit to determine *CP* observables, the data fit is repeated thousands of times while varying the given parameter according to a Gaussian function whose width corresponds to the uncertainty on the parameter. Where more than one parameter is varied (e.g. the c_i), the correlations between them are taken into account. The systematic uncertainty for each *CP* observable is taken to be the standard deviation of the fit parameter distribution from these many fits. Other systematic uncertainties are evaluated

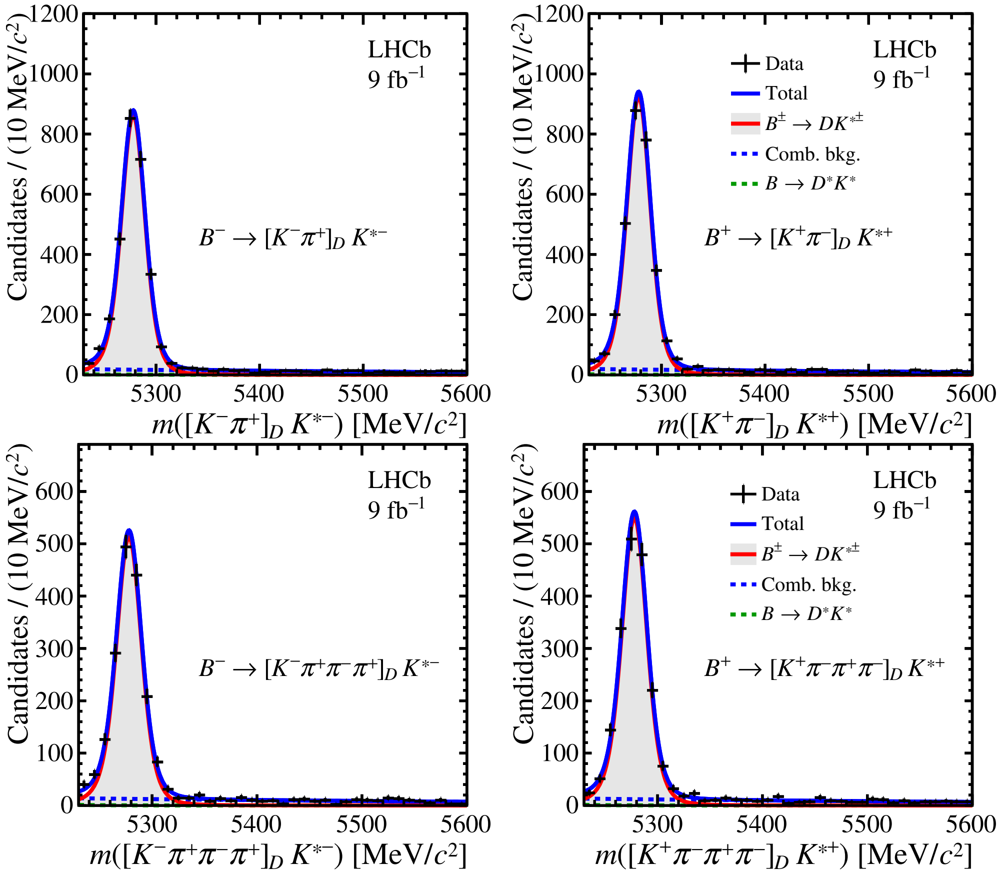

Figure 3. Reconstructed-mass (m_{rec}) distributions for the favoured (top) $K\pi$ and (bottom) $K\pi\pi\pi$ modes for (left) B^- and (right) B^+ decays, obtained with data corresponding to the full Run 1 and Run 2 datasets. Fit result is also shown.

by generating thousands of pseudoexperiments with an alternative model and fitting back with the default fit. In this case, the systematic uncertainty is computed as the difference between the generated value and the mean of the fit parameter distribution.

In the *CP* fit involving two- and four-body decays, uncertainties are assigned for the fixed values of production and detection asymmetries, branching fractions, and the ratios of selection efficiencies. Systematic uncertainties related to the signal mass model are assessed by determining the impact of the fixed parameters in the signal shape.

To assess the assumption that the slope of the combinatorial background is the same in decay modes with the same number of final-state particles, the high sideband region of m_{rec} is fitted independently for each D-meson decay mode. Pseudoexperiments are generated with the result of this fit, but fitted back with the nominal model to determine the corresponding uncertainty. Uncertainties in the yields of the PRB contribution that remain present for $m_{\text{rec}} > 5230\,\text{MeV}/c^2$ are estimated from varying the yields and shape in the initial fit. The assumption of no *CP* violation in these decays does not contribute to any significant systematic effects. The systematic uncertainties for the other backgrounds are also determined by variation of the yield and shape of each background. Due to the nature of the simultaneous fit, those backgrounds present only in certain modes have small effects on *CP* parameters that are primarily determined from other decay modes.

JHEP02(2025)113

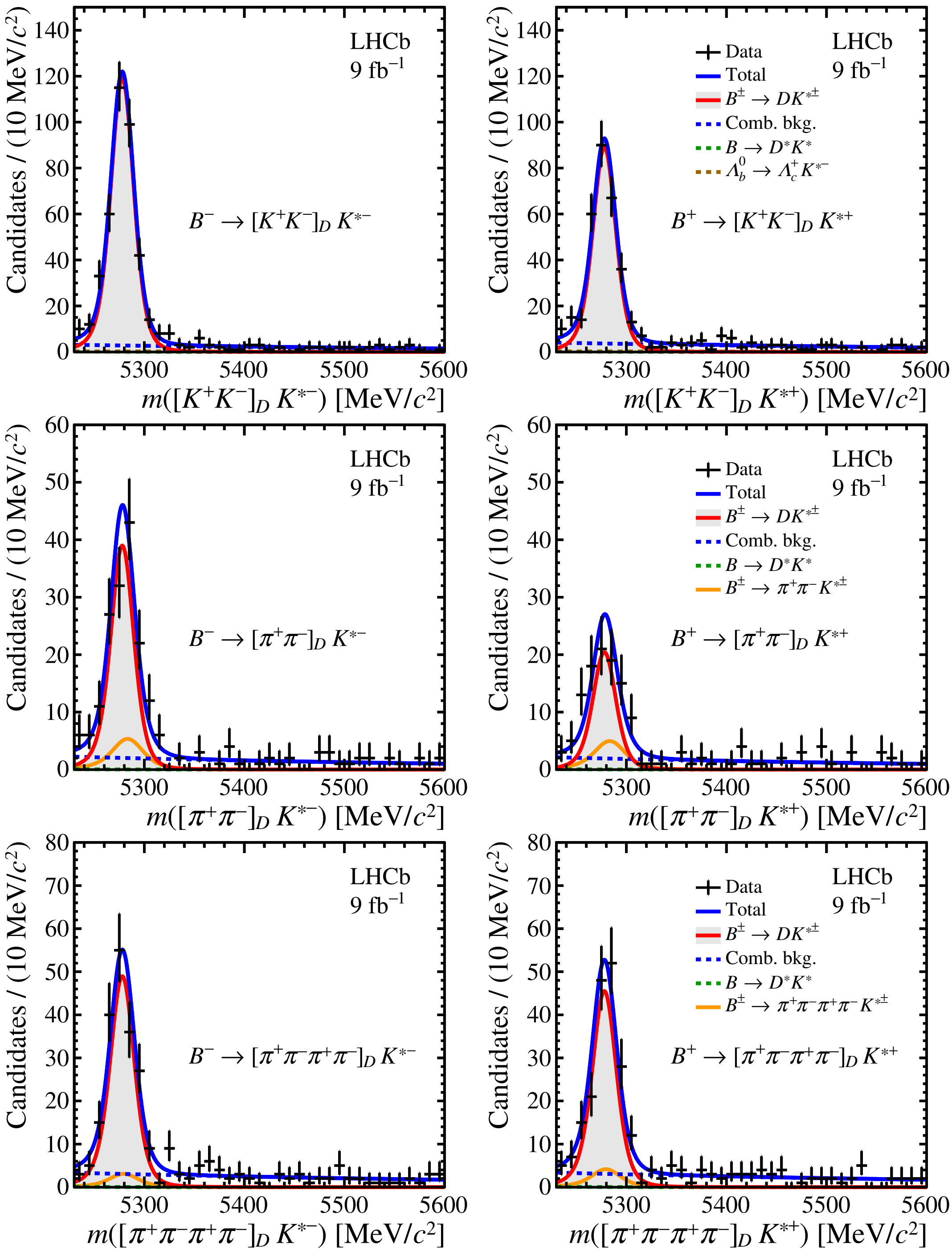

Figure 4. Reconstructed-mass ($m_{\rm rec}$) distributions for the (top row) KK, (middle row) $\pi\pi$ and (bottom row) $\pi\pi\pi\pi$ modes for (left) B^- and (right) B^+ decays, obtained with data corresponding to the full Run 1 and Run 2 datasets. Fit result is also shown.

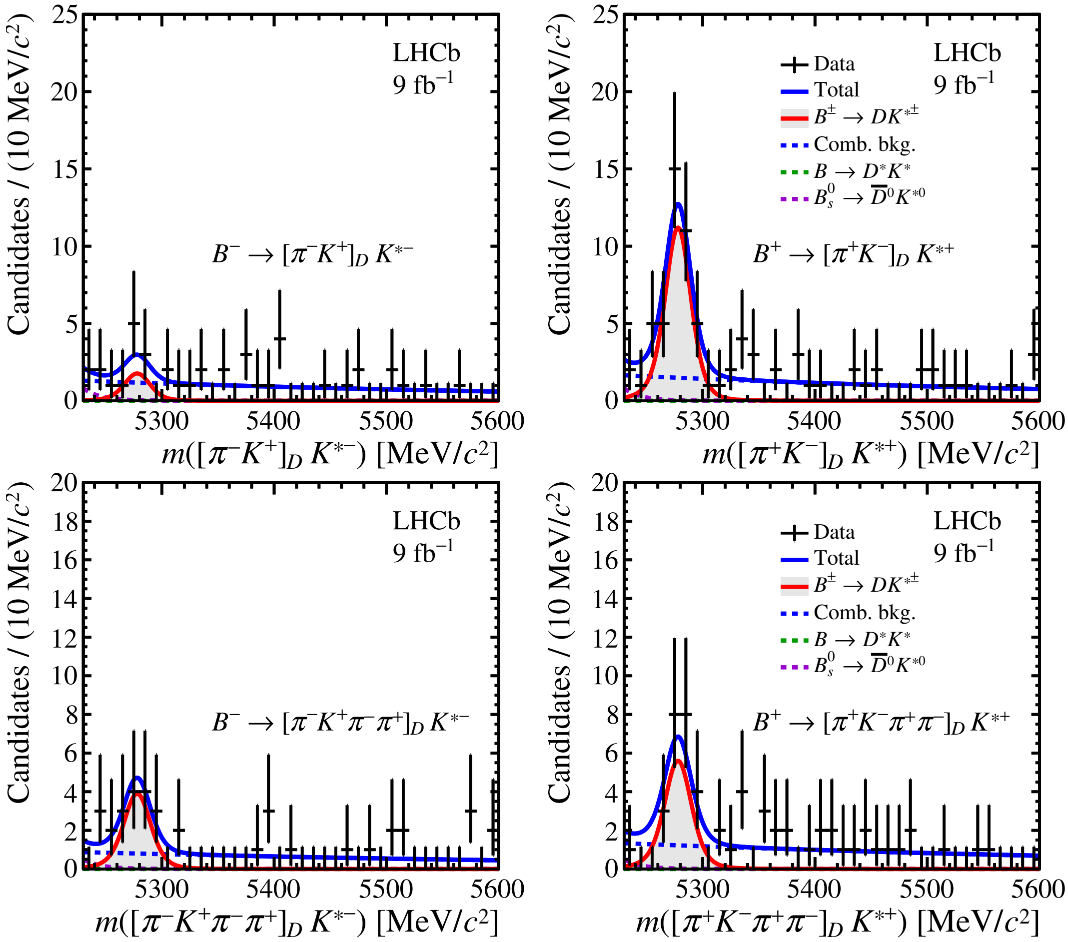

Figure 5. Reconstructed-mass ($m_{\rm rec}$) distributions for the suppressed (top row) πK and (bottom row) $\pi K\pi\pi$ modes for (left) B^- and (right) B^+ decays, obtained with data corresponding to the full Run 1 and Run 2 datasets. Fit result is also shown.

The summary of systematic uncertainties is given in table 2. In all modes except $D \to \pi\pi$ and $D \to \pi\pi\pi\pi$, the systematic uncertainty is less than 50% of the statistical one. For the $D \to \pi\pi$ and $D \to \pi\pi\pi\pi$ decay modes, the impact of the uncertainties in the charmless decays is significant. Uncertainties on the branching fractions have a large impact in the ratio observables.

In the three-body decay modes, the leading systematic uncertainty on $y_\pm$ arises from the input parameters c_i and s_i . The F_i values are also fixed in the fit and determined from $B^\pm \to D\pi^\pm$ decays. Small differences in the relative efficiency over the Dalitz plot of this control channel and the signal channel are determined in simulation. The changes are due to a looser requirement on the momentum of *long* K^0_S candidates in $B^\pm \to DK^{*\pm}$ decays at the initial stage of the selection. These changes are used to modulate the F_i values with which psuedoexperiments are generated. They are fitted with the nominal F_i values to determine the associated systematic uncertainty. This is the leading source of uncertainty on $x_\pm$.

A systematic uncertainty for the fixed value of κ is determined by generating pseudo-datasets with $\kappa \pm \sigma_\kappa$, where σ_κ is the uncertainty associated with it as determined in ref. [13],

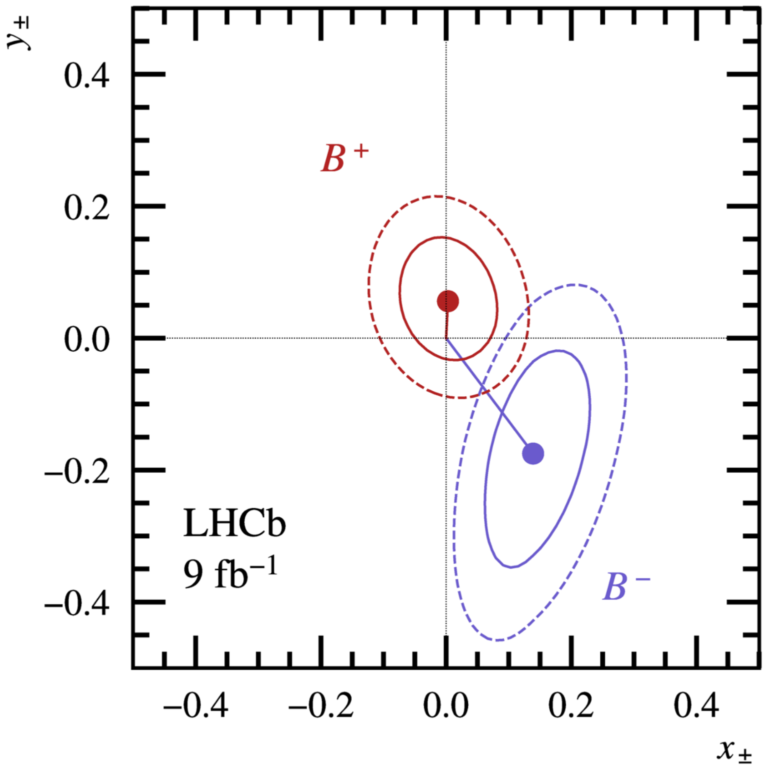

Figure 6. Central values for the measured $(x_\pm, y_\pm)$ parameters along with two-dimensional confidence regions of 68% and 95%, considering statistical uncertainty. The red (blue) contours correspond to the observables related to B^+ (B^-) decays with three-body D modes.

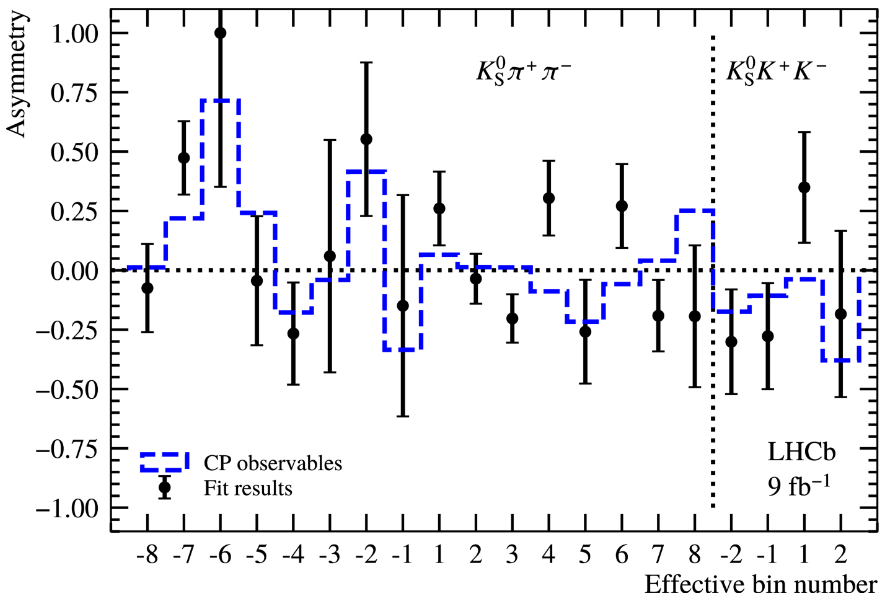

Figure 7. Raw asymmetry in each effective bin pair. It is determined using the fitted CP-violating observables (blue histogram) and the results of an alternative fit where the signal yield in each Dalitz plot bin is a free parameter (black points, with statistical uncertainties).

JHEP02(2025)113

	$A_{SS}^{K\pi}$	A_{CP}^{KK}	$A_{CP}^{\pi\pi}$	$A_{OS}^{\pi K}$	R_{CP}^{KK}	$R_{CP}^{\pi\pi}$	$R_{OS}^{\pi K}$	$A_{SS}^{K\pi\pi\pi}$	$A_{CP}^{\pi\pi\pi\pi}$	$A_{OS}^{\pi K\pi\pi}$	$R_{CP}^{\pi\pi\pi\pi}$	$R_{OS}^{\pi K\pi\pi}$
Asymmetry corrections	0.17	0.072	0.067	0.078	—	—	—	0.17	0.073	0.16	—	—
Branching fractions	—	—	—	—	0.88	1.2	—	—	—	—	3.5	—
Selection efficiencies	—	—	—	—	0.87	0.76	0.0024	—	—	—	1.2	0.0047
PID efficiencies	—	—	—	—	0.22	0.23	—	—	—	—	0.36	—
Signal shape	—	—	0.046	0.067	0.20	0.26	0.0011	—	0.020	0.069	0.31	0.0021
Combinatorial shape	0.034	0.053	0.14	2.6	0.30	0.29	0.021	0.014	0.22	0.097	0.14	0.0071
Part. reco. background	—	—	—	0.16	0.072	0.12	0.0043	—	—	—	—	—
Charmless background	—	—	4.9	0.034	—	4.5	—	—	2.9	—	3.0	—
Λ_b^0 background	—	—	0.016	0.044	0.030	0.039	—	—	—	—	—	—
B_s^0 background	0.046	0.011	0.38	1.1	0.020	0.032	0.0093	0.038	0.12	0.54	0.27	0.0054
Total systematic	0.18	0.09	4.9	2.8	1.3	4.7	0.02	0.17	2.9	0.5	4.8	0.01
Statistical	1.4	4.0	9.0	16.4	5.0	9.0	0.19	1.8	6.0	21.8	7.0	0.26

Table 2. Summary of systematic uncertainties for two- and four-body modes ($\times 10^{-2}$). Contributions which are less than 0.1% of the statistical uncertainty are not shown.

JHEP02(2025)113

	$\sigma(x_+)$	$\sigma(y_+)$	$\sigma(x_-)$	$\sigma(y_-)$
c_i, s_i uncertainty	0.4	1.9	0.9	3.9
F_i inputs	1.5	0.4	1.7	0.4
Value of κ	0.8	0.4	0.6	0.8
Efficiency correction to c_i, s_i	0.0	0.0	0.2	0.6
Bin migration	0.4	0.2	0.3	0.4
Mass model	0.1	0.1	0.1	0.3
Bias correction	0.4	0.6	0.3	0.6
Total systematic	1.8	2.1	2.1	4.1
Statistical	5.2	6.4	6.0	11.4

Table 3. Summary of systematic uncertainties for three-body modes ($\times 10^{-2}$).

and fitting them with the nominal value of 0.95. The largest deviation in the *CP* observables is taken as the systematic uncertainty. The nonuniform efficiency over the Dalitz plot can lead to a small difference between the measured values of c_i and s_i, and efficiency-corrected values. The size of the correction is estimated using simulation to provide the efficiency profile and the decay models from ref. [53] for $D \to K^0_S\pi\pi$ and ref. [54] for $D \to K^0_S KK$, and fits to pseudodatasets are used to determine the systematic uncertainty.

Migration between the Dalitz plot bins can occur due to resolution effects on the momentum of final-state particles. To first order, these effects are incorporated into the F_i values. However, second-order effects arise due to the differences in *CP* violation in $B^\pm \to D\pi^\pm$ and $B^\pm \to DK^{*\pm}$ decays. These are determined by using the momentum resolution in simulation, the *CP* violation observables of $B^\pm \to D\pi^\pm$ [55], *CP* violation observables of $B^\pm \to DK^{*\pm}$ determined in this analysis, and the D-decay model from ref. [53]. The observed differences between the two modes are used to generate pseudoexperiments which are then fit with the nominal procedure to assign the systematic uncertainty due to momentum resolution. The impact of the signal model is investigated by changing the fit function to a modified Crystal Ball [56] with different widths on both sides. This has an almost negligible impact. Removing the PRB contribution entirely has no impact on the fit results and is not considered further. Corrections to the observed bias in the fit model to measure the *CP* observables are obtained through pseudoexperiments. The dependence of this bias correction on the values of γ, δ_B, and r_B used in these simulation studies is investigated by generating alternate pseudoexperiments with varied values of γ, δ_B, and r_B. The change in bias correction values is taken as the systematic uncertainty. A summary of the systematic uncertainties in the three-body decay modes is given in table 3. The total systematic uncertainties are approximately 35% of the statistical uncertainties.

JHEP02(2025)113

9 Results and interpretation

The final results of *CP* observables for all the decay modes with statistical and systematic uncertainties are:

$$
\begin{aligned}
A_{SS}^{K\pi} &= -0.024 \pm 0.014 \pm 0.002,\\
A_{CP}^{KK} &= 0.14 \pm 0.04 \pm 0.001,\\
A_{CP}^{\pi\pi} &= 0.31 \pm 0.09 \pm 0.05,\\
A_{OS}^{\pi K} &= -0.73 \pm 0.16 \pm 0.03,\\
R_{CP}^{KK} &= 1.10 \pm 0.05 \pm 0.01,\\
R_{CP}^{\pi\pi} &= 0.96 \pm 0.09 \pm 0.05,\\
R_{OS}^{\pi K} &= 0.0098 \pm 0.0019 \pm 0.0002,\\
A_{SS}^{K\pi\pi\pi} &= -0.024 \pm 0.018 \pm 0.002,\\
A_{CP}^{\pi\pi\pi\pi} &= 0.04 \pm 0.06 \pm 0.03,\\
A_{OS}^{\pi K\pi\pi} &= -0.19 \pm 0.22 \pm 0.01,\\
R_{CP}^{\pi\pi\pi\pi} &= 1.05 \pm 0.07 \pm 0.05,\\
R_{OS}^{\pi K\pi\pi} &= 0.0118 \pm 0.0026 \pm 0.0001,\\
x_+ &= 0.003 \,{}^{+0.051}_{-0.052} \pm 0.018 \pm 0.004,\\
y_+ &= 0.056 \,{}^{+0.059}_{-0.064} \pm 0.009 \pm 0.019,\\
x_- &= 0.139 \,{}^{+0.051}_{-0.060} \pm 0.019 \pm 0.009,\\
y_- &= -0.175 \,{}^{+0.114}_{-0.103} \pm 0.013 \pm 0.039.
\end{aligned}
$$

In the case of the observables $x_\pm$ and $y_\pm$ the third uncertainty represents the propagated uncertainty from the external inputs of c_i and s_i. The correlation matrices of the statistical and systematic uncertainties are provided in the appendix. The correlations related to the strong-phase inputs are given separately.

The *CP*-violating observables from the two- and four-body decays are consistent with the previous measurement made on a partial dataset [13]. In comparison to the $B^\pm \to DK^\pm$ decay [7], the statistical precision on the *CP*-violating observables is poorer. This is due to the lower reconstruction efficiency of a $K^{*\pm}$ meson compared to a $K^\pm$ meson. However, the $B^\pm \to DK^{*\pm}$ decays provide good sensitivity due to a larger purity. In particular, there is no counterpart of misidentified background from $B^\pm \to D\pi^\pm$ as found in reconstructed $B^\pm \to DK^\pm$ candidates. In addition, the separation in $m_{\rm rec}$ between the signal and the PRB candidates is larger in this channel than in $B^\pm \to DK^\pm$, which further improves the purity.

The measured *CP*-violating observables are related to the physics parameters of interest via eqs. (2.3)–(2.8) and (2.10) in section 2. The interpretation is performed using the `GammaCombo` package [55, 57], which can implement a simple profile-likelihood method or the Feldman-Cousins approach [58] combined with a "plugin" method [59]. The correlations of statistical and systematic uncertainties for the measured *CP*-violating observables are accounted for. The *D*-decay parameters $r_D^{K\pi}$ and $\delta_D^{K\pi}$ are inputs from ref. [4], while $r_D^{K\pi\pi\pi}$, $\delta_D^{K\pi\pi\pi}$, and $\kappa^{K3\pi}$ are taken from a combination of results from BESIII, CLEO-c and LHCb collaborations [60]. Another required input is the *CP*-even fraction F_{CP} for the decay $D \to \pi\pi\pi\pi$ which is measured at BESIII [17]. The uncertainties from these input parameters

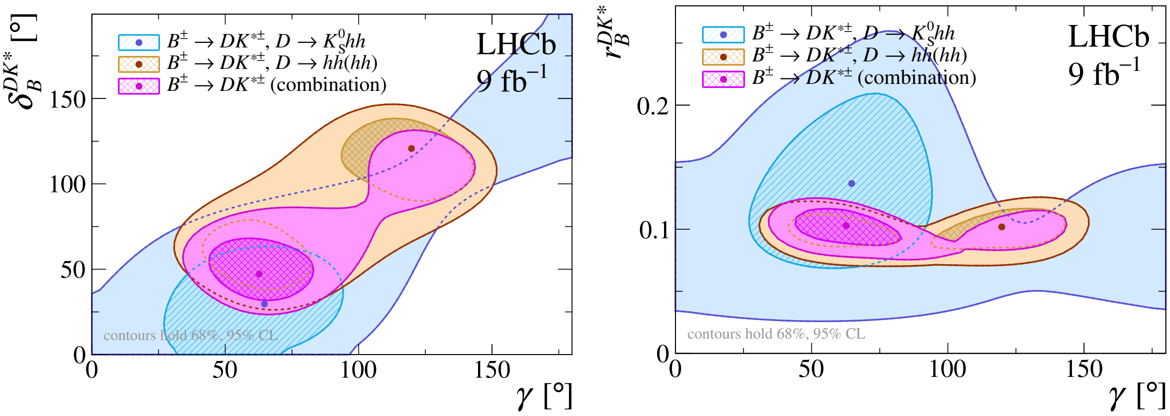

Figure 8. Two-dimensional physics parameter scans showing the contours from the combination with profile-likelihood method. Yellow, blue and magenta contours show the results for two- and four-body, three-body and all D-decay modes, respectively. The hatched and solid regions correspond to 68% and 95% confidence level, respectively.

are accounted for. The combination of the CP-violating observables from the two- and four-body decay modes leads to two solutions for γ in the range 0–180 degrees as shown in figure 8. The three-body decay modes lead to a single solution, although in two-dimensional parameter space no values of γ are excluded at the 95% confidence level. In the combination shown in figure 9, there is a single solution which is consistent with the current world average of γ. The following values of the physics parameters are found using the profile-likelihood method:

$$\begin{aligned}\gamma &= (63 \pm 13)^\circ,\\ r_B^{DK^{*\pm}} &= 0.103 \pm 0.010,\\ \delta_B^{DK^{*\pm}} &= (47^{+14}_{-12})^\circ.\end{aligned}$$

The uncertainties are found to be the same with the "plugin" method.

In summary, proton-proton collision data corresponding to an integrated luminosity of $9\,\text{fb}^{-1}$ collected by the LHCb experiment at centre-of-mass energies of $\sqrt{s} = 7$, 8 and 13 TeV is used to perform a measurement of γ using the decay $B^\pm \to DK^{*\pm}$, where the D meson decays to two-, three-, and four-body final states. The measured value is $\gamma = (63 \pm 13)^\circ$, where the uncertainty is statistically dominated. This measurement is a valuable addition to the knowledge of γ. The CP-violating observables measured here are consistent with and supersede those presented in ref. [13], and this measurement constitutes the first observation of the suppressed $B^\pm \to [\pi^\pm K^\mp]_D K^{*\pm}$ and $B^\pm \to [\pi^\pm K^\mp \pi^\pm \pi^\mp]_D K^{*\pm}$ decays.

Acknowledgments

We express our gratitude to our colleagues in the CERN accelerator departments for the excellent performance of the LHC. We thank the technical and administrative staff at the LHCb institutes. We acknowledge support from CERN and from the national agencies: CAPES, CNPq, FAPERJ and FINEP (Brazil); MOST and NSFC (China); CNRS/IN2P3 (France); BMBF, DFG and MPG (Germany); INFN (Italy); NWO (Netherlands); MNiSW

JHEP02(2025)113

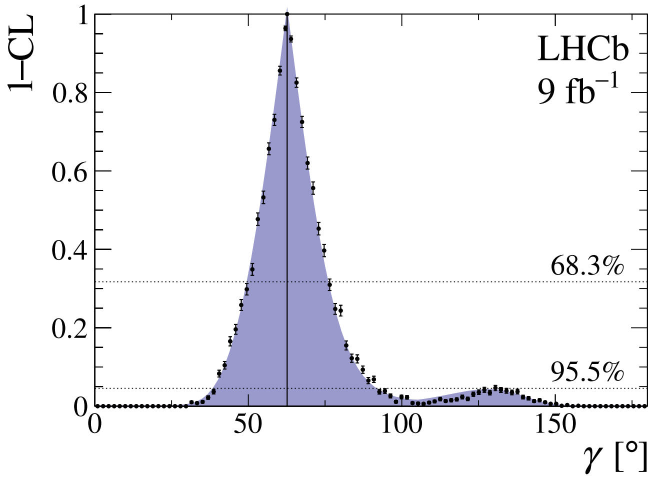

Figure 9. One-dimensional scan on the confidence limits (CL) for γ from the combination with the profile-likelihood (blue shaded region) and the plugin (black data points) methods, for all the D-decay modes. The fit result is $\gamma = (63 \pm 13)^\circ$.

and NCN (Poland); MCID/IFA (Romania); MICIU and AEI (Spain); SNSF and SER (Switzerland); NASU (Ukraine); STFC (United Kingdom); DOE NP and NSF (U.S.A.). We acknowledge the computing resources that are provided by CERN, IN2P3 (France), KIT and DESY (Germany), INFN (Italy), SURF (Netherlands), PIC (Spain), GridPP (United Kingdom), CSCS (Switzerland), IFIN-HH (Romania), CBPF (Brazil), and Polish WLCG (Poland). We are indebted to the communities behind the multiple open-source software packages on which we depend. Individual groups or members have received support from ARC and ARDC (Australia); Key Research Program of Frontier Sciences of CAS, CAS PIFI, CAS CCEPP, Fundamental Research Funds for the Central Universities, and Sci. & Tech. Program of Guangzhou (China); Minciencias (Colombia); EPLANET, Marie Skłodowska-Curie Actions, ERC and NextGenerationEU (European Union); A*MIDEX, ANR, IPhU and Labex P2IO, and Région Auvergne-Rhône-Alpes (France); AvH Foundation (Germany); ICSC (Italy); Severo Ochoa and María de Maeztu Units of Excellence, GVA, XuntaGal, GENCAT, InTalent-Inditex and Prog. Atracción Talento CM (Spain); SRC (Sweden); the Leverhulme Trust, the Royal Society and UKRI (United Kingdom).

JHEP02(2025)113

A Correlation matrices

	$A_{SS}^{K\pi}$	A_{CP}^{KK}	$A_{CP}^{\pi\pi}$	$A_{OS}^{\pi K}$	R_{CP}^{KK}	$R_{CP}^{\pi\pi}$	$R_{OS}^{\pi K}$	$A_{SS}^{K\pi\pi\pi}$	$A_{CP}^{\pi\pi\pi\pi}$	$A_{OS}^{\pi K\pi\pi}$	$R_{CP}^{\pi\pi\pi\pi}$	$R_{OS}^{\pi K\pi\pi}$
$A_{SS}^{K\pi}$	1	—	—	—	—	—	—	—	—	—	—	—
A_{CP}^{KK}		1	—	—	−0.019	—	—	—	—	—	—	—
$A_{CP}^{\pi\pi}$			1	—	—	−0.085	—	—	—	—	—	—
$A_{OS}^{\pi K}$				1	—	—	0.183	—	—	—	—	—
R_{CP}^{KK}					1	0.055	0.028	—	—	—	—	—
$R_{CP}^{\pi\pi}$						1	0.020	—	—	—	—	—
$R_{OS}^{\pi K}$							1	—	—	—	—	—
$A_{SS}^{K\pi\pi\pi}$								1	—	—	—	—
$A_{CP}^{\pi\pi\pi\pi}$									1	—	−0.022	—
$A_{OS}^{\pi K\pi\pi}$										1	—	0.040
$R_{CP}^{\pi\pi\pi\pi}$											1	0.029
$R_{OS}^{\pi K\pi\pi}$												1

Table 4. Correlation matrix of statistical uncertainties on *CP* observables for two- and four-body modes. Values below 0.1% are indicated with the symbol "–".

	$A_{SS}^{K\pi}$	A_{CP}^{KK}	$A_{CP}^{\pi\pi}$	$A_{OS}^{\pi K}$	R_{CP}^{KK}	$R_{CP}^{\pi\pi}$	$R_{OS}^{\pi K}$	$A_{SS}^{K\pi\pi\pi}$	$A_{CP}^{\pi\pi\pi\pi}$	$A_{OS}^{\pi K\pi\pi}$	$R_{CP}^{\pi\pi\pi\pi}$	$R_{OS}^{\pi K\pi\pi}$
$A_{SS}^{K\pi}$	1	0.314	—	−0.014	—	—	−0.016	0.918	0.010	−0.169	—	—
A_{CP}^{KK}		1	—	−0.017	−0.039	—	−0.011	0.319	0.032	0.155	−0.019	0.048
$A_{CP}^{\pi\pi}$			1	—	—	−0.292	—	—	—	—	—	—
$A_{OS}^{\pi K}$				1	—	—	0.220	−0.017	—	0.086	—	0.023
R_{CP}^{KK}					1	0.051	—	—	—	—	—	—
$R_{CP}^{\pi\pi}$						1	–	—	—	—	—	—
$R_{OS}^{\pi K}$							1	—	—	−0.013	—	0.063
$A_{SS}^{K\pi\pi\pi}$								1	0.013	−0.173	—	0.013
$A_{CP}^{\pi\pi\pi\pi}$									1	—	−0.605	0.025
$A_{OS}^{\pi K\pi\pi}$										1	—	0.345
$R_{CP}^{\pi\pi\pi\pi}$											1	—
$R_{OS}^{\pi K\pi\pi}$												1

Table 5. Correlation matrix of systematic uncertainties on *CP* observables for two- and four-body modes. Values below 0.1% are indicated with the symbol "–".

JHEP02(2025)113

	x_+	y_+	x_-	y_-
x_+	1	-0.144	—	—
y_+		1	—	—
x_-			1	0.448
y_-				1

Table 6. Correlation matrix of statistical uncertainties on *CP* observables for three-body modes. Values below 0.1% are indicated with the symbol "–".

	x_+	y_+	x_-	y_-
x_+	1	-0.055	0.030	0.022
y_+		1	-0.158	-0.478
x_-			1	0.319
y_-				1

Table 7. Correlation matrix of systematic uncertainties on *CP* observables for three-body modes.

	$x_-^{DK^{*+}}$	$y_-^{DK^{*+}}$	$x_+^{DK^{*+}}$	$y_+^{DK^{*+}}$
x_-^{DK}	−0.269	−0.073	0.196	−0.039
y_-^{DK}	−0.528	−0.647	−0.241	0.457
x_+^{DK}	−0.140	−0.003	−0.157	0.010
y_+^{DK}	−0.422	−0.248	0.267	−0.082
$\Re(\xi^{D\pi})$	0.013	0.275	−0.078	−0.278
$\Im(\xi^{D\pi})$	0.305	0.533	0.322	−0.534
$x_-^{DK^{*0}}$	−0.034	−0.068	−0.024	0.076
$y_-^{DK^{*0}}$	−0.028	−0.038	−0.015	0.014
$x_+^{DK^{*0}}$	0.052	0.056	0.094	−0.033
$y_+^{DK^{*0}}$	0.033	0.010	0.007	−0.015
$x_-^{D^*K}$ full reco	−0.047	−0.051	0.010	0.023
$y_-^{D^*K}$ full reco	0.022	0.022	−0.020	−0.013
$x_+^{D^*K}$ full reco	−0.033	−0.046	0.009	0.042
$y_+^{D^*K}$ full reco	−0.025	−0.048	0.029	0.024
$\Re(\xi^{D^*\pi})$ full reco	0.059	0.056	0.002	−0.022
$\Im(\xi^{D^*\pi})$ full reco	0.046	0.028	−0.013	0.011
$x_-^{D^*K}$ part reco	−0.039	−0.012	0.032	0.041
$y_-^{D^*K}$ part reco	−0.026	−0.005	0.020	0.013
$x_+^{D^*K}$ part reco	0.008	0.035	−0.040	0.002
$y_+^{D^*K}$ part reco	−0.024	−0.053	0.006	0.005
$\Re(\xi^{D^*\pi})$ part reco	−0.042	−0.018	0.013	0.020
$\Im(\xi^{D^*\pi})$ part reco	−0.044	−0.008	0.000	0.026
$x_-^{DK^{*+}}$	1.000	−0.520	0.080	0.170
$y_-^{DK^{*+}}$		1.000	−0.410	−0.560
$x_+^{DK^{*+}}$			1.000	0.760
$y_+^{DK^{*+}}$				1.000

Table 8. Correlations in the *CP* observables for the strong-phase related systematic uncertainties in three-body modes of different B-meson decay channels. The blocks of rows correspond to $B^\pm \to Dh^\pm$ [7], $B^0 \to DK^{*0}$ [61], fully reconstructed $B^\pm \to D^*h^\pm$ [62], partially reconstructed $B^\pm \to D^*h^\pm$ [63] and $B^\pm \to DK^{*\pm}$ (this analysis) channels, respectively.

JHEP02(2025)113

Data Availability Statement. This article has associated data in a data repository. Data associated to the plots in this publication as well as in supplementary materials are made available on the CERN document server at https://cds.cern.ch/record/2915477.

Code Availability Statement. This article has no associated code or the code will not be deposited.

References

[1] N. Cabibbo, *Unitary symmetry and leptonic decays*, Phys. Rev. Lett. **10** (1963) 531 [INSPIRE].

[2] M. Kobayashi and T. Maskawa, *CP violation in the renormalizable theory of weak interaction*, Prog. Theor. Phys. **49** (1973) 652 [INSPIRE].

[3] HFLAV collaboration, *Averages of b-hadron, c-hadron, and τ-lepton properties as of 2021*, Phys. Rev. D **107** (2023) 052008 [arXiv:2206.07501] [INSPIRE].

[4] LHCb collaboration, *Simultaneous determination of the CKM angle γ and parameters related to mixing and CP violation in the charm sector*, , CERN, Geneva, Switzerland (2022).

[5] J. Charles et al., *Current status of the Standard Model CKM fit and constraints on $\Delta F = 2$ new physics*, Phys. Rev. D **91** (2015) 073007 [arXiv:1501.05013] [INSPIRE].

[6] UTFIT collaboration, *New UTfit analysis of the unitarity triangle in the Cabibbo-Kobayashi-Maskawa scheme*, Rend. Lincei Sci. Fis. Nat. **34** (2023) 37 [arXiv:2212.03894] [INSPIRE].

[7] LHCb collaboration, *Measurement of the CKM angle γ in $B^\pm \to DK^\pm$ and $B^\pm \to D\pi^\pm$ decays with $D \to K^0_S h^+ h^-$*, JHEP **02** (2021) 169 [arXiv:2010.08483] [INSPIRE].

[8] LHCb collaboration, *Measurement of the CKM angle γ with $B^\pm \to D[K^\mp\pi^\pm\pi^\pm\pi^\mp]h^\pm$ decays using a binned phase-space approach*, JHEP **07** (2023) 138 [arXiv:2209.03692] [INSPIRE].

[9] LHCb collaboration, *A study of CP violation in the decays $B^\pm \to [K^+K^-\pi^+\pi^-]_D h^\pm$ $(h = K, \pi)$ and $B^\pm \to [\pi^+\pi^-\pi^+\pi^-]_D h^\pm$*, Eur. Phys. J. C **83** (2023) 547 [*Erratum ibid.* **83** (2023) 672] [arXiv:2301.10328] [INSPIRE].

[10] BELLE collaboration, *Measurement of ϕ_3 with Dalitz plot analysis of $B^+ \to D^{(*)}K^{(*)+}$ decay*, Phys. Rev. D **73** (2006) 112009 [hep-ex/0604054] [INSPIRE].

[11] BABAR collaboration, *Evidence for direct CP violation in the measurement of the Cabibbo-Kobayashi-Maskawa angle gamma with $B^\mp \to D^{(*)}K^{(*)\mp}$ decays*, Phys. Rev. Lett. **105** (2010) 121801 [arXiv:1005.1096] [INSPIRE].

[12] BABAR collaboration, *Measurement of CP violation observables and parameters for the decays $B^\pm \to DK^{*\pm}$*, Phys. Rev. D **80** (2009) 092001 [arXiv:0909.3981] [INSPIRE].

[13] LHCb collaboration, *Measurement of CP observables in $B^\pm \to DK^{*\pm}$ decays using two- and four-body D final states*, JHEP **11** (2017) 156 [*Erratum ibid.* **05** (2018) 067] [arXiv:1709.05855] [INSPIRE].

[14] M. Gronau and D. London, *How to determine all the angles of the unitarity triangle from $B^0_d \to DK_s$ and $B^0_s \to D^0$*, Phys. Lett. B **253** (1991) 483 [INSPIRE].

[15] M. Gronau and D. Wyler, *On determining a weak phase from CP asymmetries in charged B decays*, *Phys. Lett. B* **265** (1991) 172 [INSPIRE].

[16] M. Nayak et al., *First determination of the CP content of $D \to \pi^+\pi^-\pi^0$ and $D \to K^+K^-\pi^0$*, *Phys. Lett. B* **740** (2015) 1 [arXiv:1410.3964] [INSPIRE].

[17] BESIII collaborations, *Measurement of the CP-even fraction of $D^0 \to \pi^+\pi^-\pi^+\pi^-$*, *Phys. Rev. D* **106** (2022) 092004 [arXiv:2208.10098] [INSPIRE].

[18] D. Atwood, I. Dunietz and A. Soni, *Enhanced CP violation with $B \to KD^0(\bar{D}^0)$ modes and extraction of the CKM angle γ*, *Phys. Rev. Lett.* **78** (1997) 3257 [hep-ph/9612433] [INSPIRE].

[19] D. Atwood, I. Dunietz and A. Soni, *Improved methods for observing CP violation in $B^\pm \to KD$ and measuring the CKM phase γ*, *Phys. Rev. D* **63** (2001) 036005 [hep-ph/0008090] [INSPIRE].

[20] A. Bondar, *Proceedings of BINP special analysis meeting on Dalitz analysis*, unpublished, 24–26 September 2002.

[21] A. Giri, Y. Grossman, A. Soffer and J. Zupan, *Determining γ using $B^\pm \to DK^\pm$ with multibody D decays*, *Phys. Rev. D* **68** (2003) 054018 [hep-ph/0303187] [INSPIRE].

[22] BELLE collaboration, *Measurement of ϕ_3 with Dalitz plot analysis of $B^\pm \to D^{(*)}K^\pm$ decay*, *Phys. Rev. D* **70** (2004) 072003 [hep-ex/0406067] [INSPIRE].

[23] CLEO collaboration, *Model-independent determination of the strong-phase difference between D^0 and $\bar{D}^0 \to K^0_{S,L}h^+h^-$ $(h = \pi, K)$ and its impact on the measurement of the CKM angle γ/ϕ_3*, *Phys. Rev. D* **82** (2010) 112006 [arXiv:1010.2817] [INSPIRE].

[24] BESIII collaboration, *Model-independent determination of the relative strong-phase difference between D^0 and $\bar{D}^0 \to K^0_{S,L}\pi^+\pi^-$ and its impact on the measurement of the CKM angle γ/ϕ_3*, *Phys. Rev. D* **101** (2020) 112002 [arXiv:2003.00091] [INSPIRE].

[25] BESIII collaboration, *Improved model-independent determination of the strong-phase difference between D^0 and $\bar{D}^0 \to K^0_{\rm S,L}K^+K^-$ decays*, *Phys. Rev. D* **102** (2020) 052008 [arXiv:2007.07959] [INSPIRE].

[26] LHCb collaboration, *The LHCb detector at the LHC*, 2008 *JINST* **3** S08005 [INSPIRE].

[27] LHCb collaboration, *LHCb detector performance*, *Int. J. Mod. Phys. A* **30** (2015) 1530022 [arXiv:1412.6352] [INSPIRE].

[28] R. Aaij et al., *Performance of the LHCb vertex locator*, 2014 *JINST* **9** P09007 [arXiv:1405.7808] [INSPIRE].

[29] LHCB OUTER TRACKER GROUP collaboration, *Performance of the LHCb outer tracker*, 2014 *JINST* **9** P01002 [arXiv:1311.3893] [INSPIRE].

[30] LHCB OUTER TRACKER GROUP collaboration, *Improved performance of the LHCb outer tracker in LHC run 2*, 2017 *JINST* **12** P11016 [arXiv:1708.00819] [INSPIRE].

[31] LHCB RICH GROUP collaboration, *Performance of the LHCb RICH detector at the LHC*, *Eur. Phys. J. C* **73** (2013) 2431 [arXiv:1211.6759] [INSPIRE].

[32] A.A. Alves Jr. et al., *Performance of the LHCb muon system*, 2013 *JINST* **8** P02022 [arXiv:1211.1346] [INSPIRE].

[33] R. Aaij et al., *The LHCb trigger and its performance in 2011*, 2013 *JINST* **8** P04022 [arXiv:1211.3055] [INSPIRE].

[34] V.V. Gligorov and M. Williams, *Efficient, reliable and fast high-level triggering using a bonsai boosted decision tree*, 2013 *JINST* **8** P02013 [arXiv:1210.6861] [INSPIRE].

JHEP02(2025)113

[35] T. Sjöstrand, S. Mrenna and P.Z. Skands, *A brief introduction to PYTHIA 8.1*, Comput. Phys. Commun. **178** (2008) 852 [arXiv:0710.3820] [INSPIRE].

[36] LHCb collaboration, *Handling of the generation of primary events in Gauss, the LHCb simulation framework*, J. Phys. Conf. Ser. **331** (2011) 032047 [INSPIRE].

[37] D.J. Lange, *The EvtGen particle decay simulation package*, Nucl. Instrum. Meth. A **462** (2001) 152 [INSPIRE].

[38] N. Davidson, T. Przedzinski and Z. Was, *PHOTOS interface in C++: technical and physics documentation*, Comput. Phys. Commun. **199** (2016) 86 [arXiv:1011.0937] [INSPIRE].

[39] J. Allison et al., *GEANT4 developments and applications*, IEEE Trans. Nucl. Sci. **53** (2006) 270 [INSPIRE].

[40] LHCb collaboration, *The LHCb simulation application, Gauss: design, evolution and experience*, J. Phys. Conf. Ser. **331** (2011) 032023 [INSPIRE].

[41] Particle Data Group collaboration, *Review of particle physics*, Phys. Rev. D **110** (2024) 030001 [INSPIRE].

[42] W.D. Hulsbergen, *Decay chain fitting with a Kalman filter*, Nucl. Instrum. Meth. A **552** (2005) 566 [physics/0503191] [INSPIRE].

[43] L. Breiman, J. Friedman, R.A. Olshen and C.J. Stone, *Classification and regression trees*, Chapman and Hall/CRC (2017) [DOI:10.1201/9781315139470] [INSPIRE].

[44] Y. Freund and R.E. Schapire, *A decision-theoretic generalization of on-line learning and an application to boosting*, J. Comput. Syst. Sci. **55** (1997) 119 [INSPIRE].

[45] A. Blum, A. Kalai and J. Langford, *Beating the hold-out: bounds for K-fold and progressive cross-validation*, in the proceedings of the *Twelfth annual conference on computational learning theory*, (1999) [DOI:10.1145/307400.307439].

[46] LHCb collaboration, *Study of CP violation in $B^0_{(s)} \to DK^*(892)^0$ decays with $D \to K\pi(\pi\pi)$, $\pi\pi(\pi\pi)$, and KK final states*, JHEP **05** (2024) 025 [arXiv:2401.17934] [INSPIRE].

[47] LHCb collaboration, *Measurement of b-hadron production fractions in 7 TeV pp collisions*, Phys. Rev. D **85** (2012) 032008 [arXiv:1111.2357] [INSPIRE].

[48] G.A. Cowan, D.C. Craik and M.D. Needham, *RapidSim: an application for the fast simulation of heavy-quark hadron decays*, Comput. Phys. Commun. **214** (2017) 239 [arXiv:1612.07489] [INSPIRE].

[49] S.S. Wilks, *The large-sample distribution of the likelihood ratio for testing composite hypotheses*, Annals Math. Statist. **9** (1938) 60 [INSPIRE].

[50] LHCb collaboration, *Measurement of CP observables in $B^\pm \to D^{(*)}K^\pm$ and $B^\pm \to D^{(*)}\pi^\pm$ decays using two-body D final states*, JHEP **04** (2021) 081 [arXiv:2012.09903] [INSPIRE].

[51] LHCb collaboration, *Measurement of the $B^\pm$ production asymmetry and the CP asymmetry in $B^\pm \to J/\psi K^\pm$ decays*, Phys. Rev. D **95** (2017) 052005 [arXiv:1701.05501] [INSPIRE].

[52] R. Aaij et al., *Selection and processing of calibration samples to measure the particle identification performance of the LHCb experiment in run 2*, EPJ Tech. Instrum. **6** (2019) 1 [arXiv:1803.00824] [INSPIRE].

[53] BaBar and Belle collaborations, *Measurement of $\cos 2\beta$ in $B^0 \to D^{(*)}h^0$ with $D \to K^0_S\pi^+\pi^-$ decays by a combined time-dependent Dalitz plot analysis of BaBar and Belle data*, Phys. Rev. D **98** (2018) 112012 [arXiv:1804.06153] [INSPIRE].

[54] BaBar collaboration, *Measurement of D^0-$\bar{D}^0$ mixing parameters using $D^0 \to K_S^0\pi^+\pi^-$ and $D^0 \to K_S^0K^+K^-$ decays*, Phys. Rev. Lett. **105** (2010) 081803 [arXiv:1004.5053] [INSPIRE].

[55] LHCb collaboration, *Simultaneous determination of CKM angle γ and charm mixing parameters*, JHEP **12** (2021) 141 [arXiv:2110.02350] [INSPIRE].

[56] T. Skwarnicki, *A study of the radiative CASCADE transitions between the Upsilon-Prime and Upsilon resonances*, Ph.D. thesis, INP, Cracow, Poland (1986) [INSPIRE].

[57] M. Kenzie et al., *GammaCombo: a statistical analysis framework for combining measurements, fitting datasets and producing confidence intervals*, Zenodo, September 2021.

[58] G.J. Feldman and R.D. Cousins, *A unified approach to the classical statistical analysis of small signals*, Phys. Rev. D **57** (1998) 3873 [physics/9711021] [INSPIRE].

[59] S. Bodhisattva, M. Walker and M. Woodroofe, *On the unified method with nuisance parameters*, *Statist. Sinica* **19** (2009) 301 [INSPIRE].

[60] BESIII collaboration, *Measurement of the $D \to K^-\pi^+\pi^+\pi^-$ and $D \to K^-\pi^+\pi^0$ coherence factors and average strong-phase differences in quantum-correlated $D\bar{D}$ decays*, JHEP **05** (2021) 164 [arXiv:2103.05988] [INSPIRE].

[61] LHCb collaboration, *Measurement of the CKM angle γ in the $B^0 \to DK^{*0}$ channel using self-conjugate $D \to K_S^0h^+h^-$ decays*, Eur. Phys. J. C **84** (2024) 206 [arXiv:2309.05514] [INSPIRE].

[62] LHCb collaboration, *Measurement of the CKM angle γ using the $B^\pm \to D^*h^\pm$ channels*, JHEP **12** (2023) 013 [arXiv:2310.04277] [INSPIRE].

[63] LHCb collaboration, *A model-independent measurement of the CKM angle γ in partially reconstructed $B^\pm \to D^*h^\pm$ decays with $D \to K_S^0h^+h^-$ $(h = \pi, K)$*, JHEP **02** (2024) 118 [arXiv:2311.10434] [INSPIRE].

JHEP02(2025)113

The LHCb collaboration

R. Aaij[38], A.S.W. Abdelmotteleb[57], C. Abellan Beteta[51], F. Abudinén[57], T. Ackernley[61], A. A. Adefisoye[69], B. Adeva[47], M. Adinolfi[55], P. Adlarson[82], C. Agapopoulou[15], C.A. Aidala[83], Z. Ajaltouni[12], S. Akar[66], K. Akiba[38], P. Albicocco[28], J. Albrecht[20], F. Alessio[49], M. Alexander[60], Z. Aliouche[63], P. Alvarez Cartelle[56], R. Amalric[17], S. Amato[3], J.L. Amey[55], Y. Amhis[15,49], L. An[7], L. Anderlini[27], M. Andersson[51], A. Andreianov[44], P. Andreola[51], M. Andreotti[26], D. Andreou[69], A. Anelli[31,n], D. Ao[8], F. Archilli[37,t], M. Argenton[26], S. Arguedas Cuendis[10,49], A. Artamonov[44], M. Artuso[69], E. Aslanides[14], R. Ataide Da Silva[50], M. Atzeni[65], B. Audurier[16], D. Bacher[64], I. Bachiller Perea[11], S. Bachmann[22], M. Bachmayer[50], J.J. Back[57], P. Baladron Rodriguez[47], V. Balagura[16], W. Baldini[26], L. Balzani[20], H. Bao[8], J. Baptista de Souza Leite[61], C. Barbero Pretel[47], M. Barbetti[27], I. R. Barbosa[70], R.J. Barlow[63], M. Barnyakov[25], S. Barsuk[15], W. Barter[59], M. Bartolini[56], J. Bartz[69], J.M. Basels[18], S. Bashir[40], G. Bassi[35], B. Batsukh[6], P. B. Battista[15], A. Bay[50], A. Beck[57], M. Becker[20], F. Bedeschi[35], I.B. Bediaga[2], N. B. Behling[20], S. Belin[47], V. Bellee[51], K. Belous[44], I. Belov[29], I. Belyaev[36], G. Benane[14], G. Bencivenni[28], E. Ben-Haim[17], A. Berezhnoy[44], R. Bernet[51], S. Bernet Andres[45], A. Bertolin[33], C. Betancourt[51], F. Betti[59], J. Bex[56], Ia. Bezshyiko[51], J. Bhom[41], M.S. Bieker[20], N.V. Biesuz[26], P. Billoir[17], A. Biolchini[38], M. Birch[62], F.C.R. Bishop[11], A. Bitadze[63], A. Bizzeti, T. Blake[57], F. Blanc[50], J.E. Blank[20], S. Blusk[69], V. Bocharnikov[44], J.A. Boelhauve[20], O. Boente Garcia[16], T. Boettcher[66], A. Bohare[59], A. Boldyrev[44], C.S. Bolognani[79], R. Bolzonella[26,k], N. Bondar[44], A. Bordelius[49], F. Borgato[33,o], S. Borghi[63], M. Borsato[31,n], J.T. Borsuk[41], S.A. Bouchiba[50], M. Bovill[64], T.J.V. Bowcock[61], A. Boyer[49], C. Bozzi[26], A. Brea Rodriguez[50], N. Breer[20], J. Brodzicka[41], A. Brossa Gonzalo[47], J. Brown[61], D. Brundu[32], E. Buchanan[59], A. Buonaura[51], L. Buonincontri[33,o], A.T. Burke[63], C. Burr[49], J.S. Butter[56], J. Buytaert[49], W. Byczynski[49], S. Cadeddu[32], H. Cai[74], A. C. Caillet[17], R. Calabrese[26,k], S. Calderon Ramirez[10], L. Calefice[46], S. Cali[28], M. Calvi[31,n], M. Calvo Gomez[45], P. Camargo Magalhaes[2,x], J. I. Cambon Bouzas[47], P. Campana[28], D.H. Campora Perez[79], A.F. Campoverde Quezada[8], S. Capelli[31], L. Capriotti[26], R. Caravaca-Mora[10], A. Carbone[25,i], L. Carcedo Salgado[47], R. Cardinale[29,l], A. Cardini[32], P. Carniti[31,n], L. Carus[22], A. Casais Vidal[65], R. Caspary[22], G. Casse[61], J. Castro Godinez[10], M. Cattaneo[49], G. Cavallero[26,49], V. Cavallini[26,k], S. Celani[22], D. Cervenkov[64], S. Cesare[30,m], A.J. Chadwick[61], I. Chahrour[83], M. Charles[17], Ph. Charpentier[49], E. Chatzianagnostou[38], M. Chefdeville[11], C. Chen[14], S. Chen[6], Z. Chen[8], A. Chernov[41], S. Chernyshenko[53], X. Chiotopoulos[79], V. Chobanova[81], S. Cholak[50], M. Chrzaszcz[41], A. Chubykin[44], V. Chulikov[44], P. Ciambrone[28], X. Cid Vidal[47], G. Ciezarek[49], P. Cifra[49], P.E.L. Clarke[59], M. Clemencic[49], H.V. Cliff[56], J. Closier[49], C. Cocha Toapaxi[22], V. Coco[49], J. Cogan[14], E. Cogneras[12], L. Cojocariu[43], P. Collins[49], T. Colombo[49], M. C. Colonna[20], A. Comerma-Montells[46], L. Congedo[24], A. Contu[32], N. Cooke[60], I. Corredoira [47], A. Correia[17], G. Corti[49], J.J. Cottee Meldrum[55], B. Couturier[49], D.C. Craik[51], M. Cruz Torres[2,f], E. Curras Rivera[50], R. Currie[59], C.L. Da Silva[68], S. Dadabaev[44], L. Dai[71], X. Dai[7], E. Dall'Occo[20], J. Dalseno[47],

JHEP02(2025)113

C. D'Ambrosio[49], J. Daniel[12], A. Danilina[44], P. d'Argent[24], A. Davidson[57],
J.E. Davies[63], A. Davis[63], O. De Aguiar Francisco[63], C. De Angelis[32,j], F. De Benedetti[49],
J. de Boer[38], K. De Bruyn[78], S. De Capua[63], M. De Cian[22,49],
U. De Freitas Carneiro Da Graca[2,b], E. De Lucia[28], J.M. De Miranda[2], L. De Paula[3],
M. De Serio[24,g], P. De Simone[28], F. De Vellis[20], J.A. de Vries[79], F. Debernardis[24],
D. Decamp[11], V. Dedu[14], S. Dekkers[1], L. Del Buono[17], B. Delaney[65],
H.-P. Dembinski[20], J. Deng[9], V. Denysenko[51], O. Deschamps[12], F. Dettori[32,j], B. Dey[77],
P. Di Nezza[28], I. Diachkov[44], S. Didenko[44], S. Ding[69], L. Dittmann[22], V. Dobishuk[53], A. D. Docheva[60], C. Dong[5,4], A.M. Donohoe[23], F. Dordei[32], A.C. dos Reis[2], A. D. Dowling[69], W. Duan[72], P. Duda[80], M.W. Dudek[41], L. Dufour[49], V. Duk[34],
P. Durante[49], M. M. Duras[80], J.M. Durham[68], O. D. Durmus[77], A. Dziurda[41],
A. Dzyuba[44], S. Easo[58], E. Eckstein[19], U. Egede[1], A. Egorychev[44], V. Egorychev[44],
S. Eisenhardt[59], E. Ejopu[63], L. Eklund[82], M. Elashri[66], J. Ellbracht[20], S. Ely[62],
A. Ene[43], E. Epple[66], J. Eschle[69], S. Esen[22], T. Evans[63], F. Fabiano[32,j], L.N. Falcao[2],
Y. Fan[8], B. Fang[74], L. Fantini[34,p,49], M. Faria[50], K. Farmer[59], D. Fazzini[31,n],
L. Felkowski[80], M. Feng[6,8], M. Feo[20,49], A. Fernandez Casani[48], M. Fernandez Gomez[47],
A.D. Fernez[67], F. Ferrari[25], F. Ferreira Rodrigues[3], M. Ferrillo[51], M. Ferro-Luzzi[49],
S. Filippov[44], R.A. Fini[24], M. Fiorini[26,k], K.M. Fischer[64], D.S. Fitzgerald[83],
C. Fitzpatrick[63], F. Fleuret[16], M. Fontana[25], L. F. Foreman[63], R. Forty[49],
D. Foulds-Holt[56], V. Franco Lima[3], M. Franco Sevilla[67], M. Frank[49], E. Franzoso[26,k],
G. Frau[63], C. Frei[49], D.A. Friday[63], J. Fu[8], Q. Fuehring[20,56], Y. Fujii[1], T. Fulghesu[17],
E. Gabriel[38], G. Galati[24], M.D. Galati[38], A. Gallas Torreira[47], D. Galli[25,i],
S. Gambetta[59], M. Gandelman[3], P. Gandini[30], B. Ganie[63], H. Gao[8], R. Gao[64],
T.Q. Gao[56], Y. Gao[9], Y. Gao[7], Y. Gao[9], M. Garau[32,j], L.M. Garcia Martin[50],
P. Garcia Moreno[46], J. García Pardiñas[49], K. G. Garg[9], L. Garrido[46], C. Gaspar[49],
R.E. Geertsema[38], L.L. Gerken[20], E. Gersabeck[63], M. Gersabeck[63], T. Gershon[57], S. G. Ghizzo[29], Z. Ghorbanimoghaddam[55], L. Giambastiani[33,o], F. I. Giasemis[17,e], V. Gibson[56],
H.K. Giemza[42], A.L. Gilman[64], M. Giovannetti[28], A. Gioventù[46], L. Girardey[63],
P. Gironella Gironell[46], C. Giugliano[26,k], M.A. Giza[41], E.L. Gkougkousis[62],
F.C. Glaser[15,22], V.V. Gligorov[17,49], C. Göbel[70], E. Golobardes[45], D. Golubkov[44],
A. Golutvin[62,44,49], A. Gomes[2,a,†], S. Gomez Fernandez[46], F. Goncalves Abrantes[64],
M. Goncerz[41], G. Gong[5,4], J. A. Gooding[20], I.V. Gorelov[44], C. Gotti[31],
J.P. Grabowski[19], L.A. Granado Cardoso[49], E. Graugés[46], E. Graverini[50,r], L. Grazette[57],
G. Graziani, A. T. Grecu[43], L.M. Greeven[38], N.A. Grieser[66], L. Grillo[60], S. Gromov[44],
C. Gu[16], M. Guarise[26], L. Guerry[12], M. Guittiere[15], V. Guliaeva[44], P. A. Günther[22],
A.-K. Guseinov[50], E. Gushchin[44], Y. Guz[7,44,49], T. Gys[49], K. Habermann[19],
T. Hadavizadeh[1], C. Hadjivasiliou[67], G. Haefeli[50], C. Haen[49], J. Haimberger[49],
M. Hajheidari[49], G. H. Hallett[57], M.M. Halvorsen[49], P.M. Hamilton[67], J. Hammerich[61],
Q. Han[9], X. Han[22], S. Hansmann-Menzemer[22], L. Hao[8], N. Harnew[64], M. Hartmann[15],
S. Hashmi[40], J. He[8,c], F. Hemmer[49], C. Henderson[66], R.D.L. Henderson[1,57],
A.M. Hennequin[49], K. Hennessy[61], L. Henry[50], J. Herd[62], P. Herrero Gascon[22],
J. Heuel[18], A. Hicheur[3], G. Hijano Mendizabal[51], D. Hill[50], S.E. Hollitt[20], J. Horswill[63],
R. Hou[9], Y. Hou[12], N. Howarth[61], J. Hu[22], J. Hu[72], W. Hu[7], X. Hu[5,4], W. Huang[8],

JHEP02(2025)113

W. Hulsbergen[38], R.J. Hunter[57], M. Hushchyn[44], D. Hutchcroft[61], D. Ilin[44], P. Ilten[66], A. Inglessi[44], A. Iniukhin[44], A. Ishteev[44], K. Ivshin[44], R. Jacobsson[49], H. Jage[18], S.J. Jaimes Elles[48,75], S. Jakobsen[49], E. Jans[38], B.K. Jashal[48], A. Jawahery[67,49], V. Jevtic[20], E. Jiang[67], X. Jiang[6,8], Y. Jiang[8], Y. J. Jiang[7], M. John[64], A. John Rubesh Rajan[23], D. Johnson[54], C.R. Jones[56], T.P. Jones[57], S. Joshi[42], B. Jost[49], J. Juan Castella[56], N. Jurik[49], I. Juszczak[41], D. Kaminaris[50], S. Kandybei[52], M. Kane[59], Y. Kang[5,4], C. Kar[12], M. Karacson[49], D. Karpenkov[44], A. Kauniskangas[50], J.W. Kautz[66], M.K. Kazanecki[41], F. Keizer[49], M. Kenzie[56], T. Ketel[38], B. Khanji[69], A. Kharisova[44], S. Kholodenko[35,49], G. Khreich[15], T. Kirn[18], V.S. Kirsebom[31,n], O. Kitouni[65], S. Klaver[39], N. Kleijne[35,q], K. Klimaszewski[42], M.R. Kmiec[42], S. Koliiev[53], L. Kolk[20], A. Konoplyannikov[44], P. Kopciewicz[40,49], P. Koppenburg[38], M. Korolev[44], I. Kostiuk[38], O. Kot[53], S. Kotriakhova, A. Kozachuk[44], P. Kravchenko[44], L. Kravchuk[44], M. Kreps[57], P. Krokovny[44], W. Krupa[69], W. Krzemien[42], O.K. Kshyvanskyi[53], S. Kubis[80], M. Kucharczyk[41], V. Kudryavtsev[44], E. Kulikova[44], A. Kupsc[82], B. K. Kutsenko[14], D. Lacarrere[49], P. Laguarta Gonzalez[46], A. Lai[32], A. Lampis[32], D. Lancierini[56], C. Landesa Gomez[47], J.J. Lane[1], R. Lane[55], G. Lanfranchi[28], C. Langenbruch[22], J. Langer[20], O. Lantwin[44], T. Latham[57], F. Lazzari[35,r], C. Lazzeroni[54], R. Le Gac[14], H. Lee[61], R. Lefèvre[12], A. Leflat[44], S. Legotin[44], M. Lehuraux[57], E. Lemos Cid[49], O. Leroy[14], T. Lesiak[41], E. Lesser[49], B. Leverington[22], A. Li[5,4], C. Li[14], H. Li[72], K. Li[9], L. Li[63], M. Li[9], P. Li[8], P.-R. Li[73], Q. Li[6,8], S. Li[9], T. Li[6,d], T. Li[72], Y. Li[9], Y. Li[6], Z. Lian[5,4], X. Liang[69], S. Libralon[48], C. Lin[8], T. Lin[58], R. Lindner[49], V. Lisovskyi[50], R. Litvinov[32,49], F. L. Liu[1], G. Liu[72], K. Liu[73], S. Liu[6,8], W. Liu[9], Y. Liu[59], Y. Liu[73], Y. L. Liu[62], A. Lobo Salvia[46], A. Loi[32], J. Lomba Castro[47], T. Long[56], J.H. Lopes[3], A. Lopez Huertas[46], S. López Soliño[47], Q. Lu[16], C. Lucarelli[27], D. Lucchesi[33,o], M. Lucio Martinez[79], V. Lukashenko[38,53], Y. Luo[7], A. Lupato[33,h], E. Luppi[26,k], K. Lynch[23], X.-R. Lyu[8], G. M. Ma[5,4], R. Ma[8], S. Maccolini[20], F. Machefert[15], F. Maciuc[43], B. Mack[69], I. Mackay[64], L. M. Mackey[69], L.R. Madhan Mohan[56], M. M. Madurai[54], A. Maevskiy[44], D. Magdalinski[38], D. Maisuzenko[44], M.W. Majewski[40], J.J. Malczewski[41], S. Malde[64], L. Malentacca[49], A. Malinin[44], T. Maltsev[44], G. Manca[32,j], G. Mancinelli[14], C. Mancuso[30,15,m], R. Manera Escalero[46], D. Manuzzi[25], D. Marangotto[30,m], J.F. Marchand[11], R. Marchevski[50], U. Marconi[25], E. Mariani[17], S. Mariani[49], C. Marin Benito[46], J. Marks[22], A.M. Marshall[55], L. Martel[64], G. Martelli[34,p], G. Martellotti[36], L. Martinazzoli[49], M. Martinelli[31,n], D. Martinez Santos[47], F. Martinez Vidal[48], A. Massafferri[2], R. Matev[49], A. Mathad[49], V. Matiunin[44], C. Matteuzzi[69], K.R. Mattioli[16], A. Mauri[62], E. Maurice[16], J. Mauricio[46], P. Mayencourt[50], J. Mazorra de Cos[48], M. Mazurek[42], M. McCann[62], L. Mcconnell[23], T.H. McGrath[63], N.T. McHugh[60], A. McNab[63], R. McNulty[23], B. Meadows[66], G. Meier[20], D. Melnychuk[42], F. M. Meng[5,4], M. Merk[38,79], A. Merli[50], L. Meyer Garcia[67], D. Miao[6,8], H. Miao[8], M. Mikhasenko[76], D.A. Milanes[75], A. Minotti[31], E. Minucci[69], T. Miralles[12], B. Mitreska[20], D.S. Mitzel[20], A. Modak[58], R.A. Mohammed[64], R.D. Moise[18], S. Mokhnenko[44], E. F. Molina Cardenas[83], T. Mombächer[49], M. Monk[57,1], S. Monteil[12], A. Morcillo Gomez[47], G. Morello[28], M.J. Morello[35,q], M.P. Morgenthaler[22], A.B. Morris[49], A.G. Morris[14], R. Mountain[69],

H. Mu[5,4], Z. M. Mu[7], E. Muhammad[57], F. Muheim[59], M. Mulder[78], K. Müller[51], F. Muñoz-Rojas[10], R. Murta[62], P. Naik[61], T. Nakada[50], R. Nandakumar[58], T. Nanut[49], I. Nasteva[3], M. Needham[59], N. Neri[30,m], S. Neubert[19], N. Neufeld[49], P. Neustroev[44], J. Nicolini[20,15], D. Nicotra[79], E.M. Niel[50], N. Nikitin[44], P. Nogarolli[3], P. Nogga[19], C. Normand[55], J. Novoa Fernandez[47], G. Nowak[66], C. Nunez[83], H. N. Nur[60], A. Oblakowska-Mucha[40], V. Obraztsov[44], T. Oeser[18], S. Okamura[26,k], A. Okhotnikov[44], O. Okhrimenko[53], R. Oldeman[32,j], F. Oliva[59], M. Olocco[20], C.J.G. Onderwater[79], R.H. O'Neil[59], D. Osthues[20], J.M. Otalora Goicochea[3], P. Owen[51], A. Oyanguren[48], O. Ozcelik[59], F. Paciolla[35,u], A. Padee[42], K.O. Padeken[19], B. Pagare[57], P.R. Pais[22], T. Pajero[49], A. Palano[24], M. Palutan[28], G. Panshin[44], L. Paolucci[57], A. Papanestis[58,49], M. Pappagallo[24,g], L.L. Pappalardo[26,k], C. Pappenheimer[66], C. Parkes[63], B. Passalacqua[26], G. Passaleva[27], D. Passaro[35,q], A. Pastore[24], M. Patel[62], J. Patoc[64], C. Patrignani[25,i], A. Paul[69], C.J. Pawley[79], A. Pellegrino[38], J. Peng[6,8], M. Pepe Altarelli[28], S. Perazzini[25], D. Pereima[44], H. Pereira Da Costa[68], A. Pereiro Castro[47], P. Perret[12], A. Perro[49], K. Petridis[55], A. Petrolini[29,l], J. P. Pfaller[66], H. Pham[69], L. Pica[35], M. Piccini[34], L. Piccolo[32], B. Pietrzyk[11], G. Pietrzyk[15], D. Pinci[36], F. Pisani[49], M. Pizzichemi[31,n], V. Placinta[43], M. Plo Casasus[47], T. Poeschl[49], F. Polci[17,49], M. Poli Lener[28], A. Poluektov[14], N. Polukhina[44], I. Polyakov[44], E. Polycarpo[3], S. Ponce[49], D. Popov[8], S. Poslavskii[44], K. Prasanth[59], C. Prouve[47], D. P. Provenzano[32], V. Pugatch[53], G. Punzi[35,r], S. Qasim[51], Q. Q. Qian[7], W. Qian[8], N. Qin[5,4], S. Qu[5,4], R. Quagliani[49], R.I. Rabadan Trejo[57], J.H. Rademacker[55], M. Rama[35], M. Ramírez García[83], V. Ramos De Oliveira[70], M. Ramos Pernas[57], M.S. Rangel[3], F. Ratnikov[44], G. Raven[39], M. Rebollo De Miguel[48], F. Redi[30,h], J. Reich[55], F. Reiss[63], Z. Ren[8], P.K. Resmi[64], R. Ribatti[50], G. R. Ricart[16,13], D. Riccardi[35,q], S. Ricciardi[58], K. Richardson[65], M. Richardson-Slipper[59], K. Rinnert[61], P. Robbe[15], G. Robertson[60], E. Rodrigues[61], E. Rodriguez Fernandez[47], J.A. Rodriguez Lopez[75], E. Rodriguez Rodriguez[47], J. Roensch[20], A. Rogachev[44], A. Rogovskiy[58], D.L. Rolf[49], P. Roloff[49], V. Romanovskiy[66], M. Romero Lamas[47], A. Romero Vidal[47], G. Romolini[26], F. Ronchetti[50], T. Rong[7], M. Rotondo[28], S. R. Roy[22], M.S. Rudolph[69], M. Ruiz Diaz[22], R.A. Ruiz Fernandez[47], J. Ruiz Vidal[82,y], A. Ryzhikov[44], J. Ryzka[40], J. J. Saavedra-Arias[10], J.J. Saborido Silva[47], R. Sadek[16], N. Sagidova[44], D. Sahoo[77], N. Sahoo[54], B. Saitta[32,j], M. Salomoni[31,n,49], I. Sanderswood[48], R. Santacesaria[36], C. Santamarina Rios[47], M. Santimaria[28,49], L. Santoro[2], E. Santovetti[37], A. Saputi[26,49], D. Saranin[44], A. S. Sarnatskiy[78], G. Sarpis[59], M. Sarpis[63], C. Satriano[36,s], A. Satta[37], M. Saur[7], D. Savrina[44], H. Sazak[18], L.G. Scantlebury Smead[64], A. Scarabotto[20], S. Schael[18], S. Scherl[61], M. Schiller[60], H. Schindler[49], M. Schmelling[21], B. Schmidt[49], S. Schmitt[18], H. Schmitz[19], O. Schneider[50], A. Schopper[49], N. Schulte[20], S. Schulte[50], M.H. Schune[15], R. Schwemmer[49], G. Schwering[18], B. Sciascia[28], A. Sciuccati[49], S. Sellam[47], A. Semennikov[44], T. Senger[51], M. Senghi Soares[39], A. Sergi[29,49], N. Serra[51], L. Sestini[33], A. Seuthe[20], Y. Shang[7], D.M. Shangase[83], M. Shapkin[44], R. S. Sharma[69], I. Shchemerov[44], L. Shchutska[50], T. Shears[61], L. Shekhtman[44], Z. Shen[7], S. Sheng[6,8], V. Shevchenko[44], B. Shi[8], Q. Shi[8], Y. Shimizu[15], E. Shmanin[25], R. Shorkin[44], J.D. Shupperd[69], R. Silva Coutinho[69], G. Simi[33,o], S. Simone[24,g], N. Skidmore[57],

JHEP02(2025)113

T. Skwarnicki[69], M.W. Slater[54], J.C. Smallwood[64], E. Smith[65], K. Smith[68], M. Smith[62], A. Snoch[38], L. Soares Lavra[59], M.D. Sokoloff[66], F.J.P. Soler[60], A. Solomin[44,55], A. Solovev[44], I. Solovyev[44], R. Song[1], Y. Song[50], Y. Song[5,4], Y. S. Song[7], F.L. Souza De Almeida[69], B. Souza De Paula[3], E. Spadaro Norella[29], E. Spedicato[25], J.G. Speer[20], E. Spiridenkov[44], P. Spradlin[60], V. Sriskaran[49], F. Stagni[49], M. Stahl[49], S. Stahl[49], S. Stanislaus[64], E.N. Stein[49], O. Steinkamp[51], O. Stenyakin[44], H. Stevens[20], D. Strekalina[44], Y. Su[8], F. Suljik[64], J. Sun[32], L. Sun[74], Y. Sun[67], D. S. Sundfeld Lima[2], W. Sutcliffe[51], P.N. Swallow[54], F. Swystun[56], A. Szabelski[42], T. Szumlak[40], Y. Tan[5,4], M.D. Tat[64], A. Terentev[44], F. Terzuoli[35,u,49], F. Teubert[49], E. Thomas[49], D.J.D. Thompson[54], H. Tilquin[62], V. Tisserand[12], S. T'Jampens[11], M. Tobin[6,49], L. Tomassetti[26,k], G. Tonani[30,m,49], X. Tong[7], D. Torres Machado[2], L. Toscano[20], D.Y. Tou[5,4], C. Trippl[45], G. Tuci[22], N. Tuning[38], L.H. Uecker[22], A. Ukleja[40], D.J. Unverzagt[22], E. Ursov[44], A. Usachov[39], A. Ustyuzhanin[44], U. Uwer[22], V. Vagnoni[25], V. Valcarce Cadenas[47], G. Valenti[25], N. Valls Canudas[49], H. Van Hecke[68], E. van Herwijnen[62], C.B. Van Hulse[47,w], R. Van Laak[50], M. van Veghel[38], G. Vasquez[51], R. Vazquez Gomez[46], P. Vazquez Regueiro[47], C. Vázquez Sierra[47], S. Vecchi[26], J.J. Velthuis[55], M. Veltri[27,v], A. Venkateswaran[50], M. Verdoglia[32], M. Vesterinen[57], D. Vico Benet[64], P. V. Vidrier Villalba[46], M. Vieites Diaz[49], X. Vilasis-Cardona[45], E. Vilella Figueras[61], A. Villa[25], P. Vincent[17], F.C. Volle[54], D. vom Bruch[14], N. Voropaev[44], K. Vos[79], G. Vouters[11], C. Vrahas[59], J. Wagner[20], J. Walsh[35], E.J. Walton[1,57], G. Wan[7], C. Wang[22], G. Wang[9], J. Wang[7], J. Wang[6], J. Wang[5,4], J. Wang[74], M. Wang[30], N. W. Wang[8], R. Wang[55], X. Wang[9], X. Wang[72], X. W. Wang[62], Y. Wang[7], Z. Wang[15], Z. Wang[5,4], Z. Wang[30], J.A. Ward[57,1], M. Waterlaat[49], N.K. Watson[54], D. Websdale[62], Y. Wei[7], J. Wendel[81], B.D.C. Westhenry[55], C. White[56], M. Whitehead[60], E. Whiter[54], A.R. Wiederhold[63], D. Wiedner[20], G. Wilkinson[64], M.K. Wilkinson[66], M. Williams[65], M.R.J. Williams[59], R. Williams[56], Z. Williams[55], F.F. Wilson[58], W. Wislicki[42], M. Witek[41], L. Witola[22], G. Wormser[15], S.A. Wotton[56], H. Wu[69], J. Wu[9], Y. Wu[7], K. Wyllie[49], S. Xian[72], Z. Xiang[6], Y. Xie[9], A. Xu[35], J. Xu[8], L. Xu[5,4], L. Xu[5,4], M. Xu[57], Z. Xu[49], Z. Xu[8], Z. Xu[6], D. Yang[5], K. Yang[62], S. Yang[8], X. Yang[7], Y. Yang[29,l], Z. Yang[7], Z. Yang[67], V. Yeroshenko[15], H. Yeung[63], H. Yin[9], C. Y. Yu[7], J. Yu[71], X. Yuan[6], Y Yuan[6,8], E. Zaffaroni[50], M. Zavertyaev[21], M. Zdybal[41], C. Zeng[6,8], M. Zeng[5,4], C. Zhang[7], D. Zhang[9], J. Zhang[8], L. Zhang[5,4], S. Zhang[71], S. Zhang[64], Y. Zhang[7], Y. Z. Zhang[5,4], Y. Zhao[22], A. Zharkova[44], A. Zhelezov[22], S. Z. Zheng[7], X. Z. Zheng[5,4], Y. Zheng[8], T. Zhou[7], X. Zhou[9], Y. Zhou[8], V. Zhovkovska[57], L. Z. Zhu[8], X. Zhu[5,4], X. Zhu[9], V. Zhukov[18], J. Zhuo[48], Q. Zou[6,8], D. Zuliani[33,o], G. Zunica[50]

[1] *School of Physics and Astronomy, Monash University, Melbourne, Australia*
[2] *Centro Brasileiro de Pesquisas Físicas (CBPF), Rio de Janeiro, Brazil*
[3] *Universidade Federal do Rio de Janeiro (UFRJ), Rio de Janeiro, Brazil*
[4] *Center for High Energy Physics, Tsinghua University, Beijing, China*
[5] *Department of Engineering Physics, Tsinghua University, Beijing, China, Beijing, China*
[6] *Institute Of High Energy Physics (IHEP), Beijing, China*
[7] *School of Physics State Key Laboratory of Nuclear Physics and Technology, Peking University, Beijing, China*

JHEP02(2025)113

[8] *University of Chinese Academy of Sciences, Beijing, China*
[9] *Institute of Particle Physics, Central China Normal University, Wuhan, Hubei, China*
[10] *Consejo Nacional de Rectores (CONARE), San Jose, Costa Rica*
[11] *Université Savoie Mont Blanc, CNRS, IN2P3-LAPP, Annecy, France*
[12] *Université Clermont Auvergne, CNRS/IN2P3, LPC, Clermont-Ferrand, France*
[13] *Departement de Physique Nucleaire (SPhN), Gif-Sur-Yvette, France*
[14] *Aix Marseille Univ, CNRS/IN2P3, CPPM, Marseille, France*
[15] *Université Paris-Saclay, CNRS/IN2P3, IJCLab, Orsay, France*
[16] *Laboratoire Leprince-Ringuet, CNRS/IN2P3, Ecole Polytechnique, Institut Polytechnique de Paris, Palaiseau, France*
[17] *LPNHE, Sorbonne Université, Paris Diderot Sorbonne Paris Cité, CNRS/IN2P3, Paris, France*
[18] *I. Physikalisches Institut, RWTH Aachen University, Aachen, Germany*
[19] *Universität Bonn — Helmholtz-Institut für Strahlen und Kernphysik, Bonn, Germany*
[20] *Fakultät Physik, Technische Universität Dortmund, Dortmund, Germany*
[21] *Max-Planck-Institut für Kernphysik (MPIK), Heidelberg, Germany*
[22] *Physikalisches Institut, Ruprecht-Karls-Universität Heidelberg, Heidelberg, Germany*
[23] *School of Physics, University College Dublin, Dublin, Ireland*
[24] *INFN Sezione di Bari, Bari, Italy*
[25] *INFN Sezione di Bologna, Bologna, Italy*
[26] *INFN Sezione di Ferrara, Ferrara, Italy*
[27] *INFN Sezione di Firenze, Firenze, Italy*
[28] *INFN Laboratori Nazionali di Frascati, Frascati, Italy*
[29] *INFN Sezione di Genova, Genova, Italy*
[30] *INFN Sezione di Milano, Milano, Italy*
[31] *INFN Sezione di Milano-Bicocca, Milano, Italy*
[32] *INFN Sezione di Cagliari, Monserrato, Italy*
[33] *INFN Sezione di Padova, Padova, Italy*
[34] *INFN Sezione di Perugia, Perugia, Italy*
[35] *INFN Sezione di Pisa, Pisa, Italy*
[36] *INFN Sezione di Roma La Sapienza, Roma, Italy*
[37] *INFN Sezione di Roma Tor Vergata, Roma, Italy*
[38] *Nikhef National Institute for Subatomic Physics, Amsterdam, Netherlands*
[39] *Nikhef National Institute for Subatomic Physics and VU University Amsterdam, Amsterdam, Netherlands*
[40] *AGH — University of Krakow, Faculty of Physics and Applied Computer Science, Kraków, Poland*
[41] *Henryk Niewodniczanski Institute of Nuclear Physics Polish Academy of Sciences, Kraków, Poland*
[42] *National Center for Nuclear Research (NCBJ), Warsaw, Poland*
[43] *Horia Hulubei National Institute of Physics and Nuclear Engineering, Bucharest-Magurele, Romania*
[44] *Affiliated with an institute covered by a cooperation agreement with CERN*
[45] *DS4DS, La Salle, Universitat Ramon Llull, Barcelona, Spain*
[46] *ICCUB, Universitat de Barcelona, Barcelona, Spain*
[47] *Instituto Galego de Física de Altas Enerxías (IGFAE), Universidade de Santiago de Compostela, Santiago de Compostela, Spain*
[48] *Instituto de Fisica Corpuscular, Centro Mixto Universidad de Valencia — CSIC, Valencia, Spain*
[49] *European Organization for Nuclear Research (CERN), Geneva, Switzerland*
[50] *Institute of Physics, Ecole Polytechnique Fédérale de Lausanne (EPFL), Lausanne, Switzerland*
[51] *Physik-Institut, Universität Zürich, Zürich, Switzerland*
[52] *NSC Kharkiv Institute of Physics and Technology (NSC KIPT), Kharkiv, Ukraine*
[53] *Institute for Nuclear Research of the National Academy of Sciences (KINR), Kyiv, Ukraine*
[54] *University of Birmingham, Birmingham, United Kingdom*
[55] *H.H. Wills Physics Laboratory, University of Bristol, Bristol, United Kingdom*
[56] *Cavendish Laboratory, University of Cambridge, Cambridge, United Kingdom*
[57] *Department of Physics, University of Warwick, Coventry, United Kingdom*
[58] *STFC Rutherford Appleton Laboratory, Didcot, United Kingdom*

JHEP02(2025)113

[59] School of Physics and Astronomy, University of Edinburgh, Edinburgh, United Kingdom
[60] School of Physics and Astronomy, University of Glasgow, Glasgow, United Kingdom
[61] Oliver Lodge Laboratory, University of Liverpool, Liverpool, United Kingdom
[62] Imperial College London, London, United Kingdom
[63] Department of Physics and Astronomy, University of Manchester, Manchester, United Kingdom
[64] Department of Physics, University of Oxford, Oxford, United Kingdom
[65] Massachusetts Institute of Technology, Cambridge, MA, United States
[66] University of Cincinnati, Cincinnati, OH, United States
[67] University of Maryland, College Park, MD, United States
[68] Los Alamos National Laboratory (LANL), Los Alamos, NM, United States
[69] Syracuse University, Syracuse, NY, United States
[70] Pontifícia Universidade Católica do Rio de Janeiro (PUC-Rio), Rio de Janeiro, Brazil, associated to [3]
[71] School of Physics and Electronics, Hunan University, Changsha City, China, associated to [9]
[72] Guangdong Provincial Key Laboratory of Nuclear Science, Guangdong-Hong Kong Joint Laboratory of Quantum Matter, Institute of Quantum Matter, South China Normal University, Guangzhou, China, associated to [4]
[73] Lanzhou University, Lanzhou, China, associated to [6]
[74] School of Physics and Technology, Wuhan University, Wuhan, China, associated to [4]
[75] Departamento de Fisica, Universidad Nacional de Colombia, Bogota, Colombia, associated to [17]
[76] Ruhr Universitaet Bochum, Fakultaet f. Physik und Astronomie, Bochum, Germany, associated to [20]
[77] Eotvos Lorand University, Budapest, Hungary, associated to [49]
[78] Van Swinderen Institute, University of Groningen, Groningen, Netherlands, associated to [38]
[79] Universiteit Maastricht, Maastricht, Netherlands, associated to [38]
[80] Tadeusz Kosciuszko Cracow University of Technology, Cracow, Poland, associated to [41]
[81] Universidade da Coruña, A Coruna, Spain, associated to [45]
[82] Department of Physics and Astronomy, Uppsala University, Uppsala, Sweden, associated to [60]
[83] University of Michigan, Ann Arbor, MI, United States, associated to [69]

[a] Universidade de Brasília, Brasília, Brazil
[b] Centro Federal de Educacão Tecnológica Celso Suckow da Fonseca, Rio De Janeiro, Brazil
[c] Hangzhou Institute for Advanced Study, UCAS, Hangzhou, China
[d] School of Physics and Electronics, Henan University, Kaifeng, China
[e] LIP6, Sorbonne Université, Paris, France
[f] Universidad Nacional Autónoma de Honduras, Tegucigalpa, Honduras
[g] Università di Bari, Bari, Italy
[h] Universita degli studi di Bergamo, Bergamo, Italy
[i] Università di Bologna, Bologna, Italy
[j] Università di Cagliari, Cagliari, Italy
[k] Università di Ferrara, Ferrara, Italy
[l] Università di Genova, Genova, Italy
[m] Università degli Studi di Milano, Milano, Italy
[n] Università degli Studi di Milano-Bicocca, Milano, Italy
[o] Università di Padova, Padova, Italy
[p] Università di Perugia, Perugia, Italy
[q] Scuola Normale Superiore, Pisa, Italy
[r] Università di Pisa, Pisa, Italy
[s] Università della Basilicata, Potenza, Italy
[t] Università di Roma Tor Vergata, Roma, Italy
[u] Università di Siena, Siena, Italy
[v] Università di Urbino, Urbino, Italy
[w] Universidad de Alcalá, Alcalá de Henares, Spain
[x] Facultad de Ciencias Fisicas, Madrid, Spain
[y] Department of Physics/Division of Particle Physics, Lund, Sweden
[†] Deceased

JHEP02(2025)113